

1 **Investigating the response of China's surface ozone**
2 **concentration to the future changes of multiple factors**

3

4 Jinya Yang¹, Yutong Wang¹, Lei Zhang^{1,2}, Yu Zhao^{1,2*}

5

6 1. State Key Laboratory of Pollution Control and Resource Reuse, School of
7 Environment, Nanjing University, 163 Xianlin Rd., Nanjing, Jiangsu 210023, China

8 2. Jiangsu Collaborative Innovation Center of Atmospheric Environment and
9 Equipment Technology (CICAEET), Nanjing University of Information Science and
10 Technology, Jiangsu 210044, China

11

12 *Corresponding author: Yu Zhao

13 Phone: 86-25-89680650; email: yuzhao@nju.edu.cn

14

15 **Abstract**

16 Climate change and associated human response are supposed to greatly alter
17 surface ozone (O₃), an air pollutant generated through photochemical reactions
18 involving both anthropogenic and biogenic precursors. However, a comprehensive
19 evaluation of China's O₃ response to these multiple changes has been lacking. We
20 present a modelling framework under Shared Socioeconomic Pathways (SSP2-45),
21 incorporating future changes in local and foreign anthropogenic emissions,
22 meteorological conditions, and BVOCs emissions. From the 2020s to 2060s, daily
23 maximum 8-hour average (MDA8) O₃ concentration is simulated to decline by 7.7
24 ppb in the warm season (April-September) and 1.1 ppb in non-warm season
25 (October-March) over the country, with a substantial reduction in exceedances of
26 national O₃ standards. Notably, O₃ decreases are more pronounced in developed
27 regions such as BTH, YRD, and PRD during warm season, with reductions of 9.7,
28 14.8, and 12.5 ppb, respectively. Conversely, in non-warm season, the MDA8 O₃ in
29 BTH and YRD will increase by 5.4-5 and 3.4-3 ppb, partly attributed to reduced NO_x
30 emissions and thereby weakened titration effect. O₃ pollution will thus expand into
31 the non-warm season in the future. Sensitivity analyses reveal that local emission
32 change will predominantly influence future O₃ distribution and magnitude, with
33 contributions from other factors within ±25 %. Furthermore, the joint impact of
34 multiple factors on O₃ reduction will be larger than the sum of individual factors, due
35 to changes in the O₃ formation regime. This study highlights the necessity of
36 region-specific emission control strategies to mitigate potential O₃ increases during
37 non-warm season and under climate penalty.

38 **1 Introduction**

39 Surface ozone (O₃) is a secondary air pollutant generated by photochemical
40 reactions in the presence of two main kinds of precursors NO_x (NO_x=NO+NO₂) and
41 volatile organic compounds (VOCs). It has been reported to be a non-negligible threat

42 to both human health and crop yield, and also a short-lived climate forcer with
43 warming effect (Finlaysonpitts and Pitts, 1997; Jerrett et al., 2009; Avnery et al., 2011;
44 [Lelieveld et al., 2015](#); von Schneidemesser et al., 2015; Tai and Val Martin, 2017;
45 [Yin et al., 2020](#); Feng et al., 2022; [Niu et al., 2022](#)). Given the abundant emissions of
46 anthropogenic NO_x and VOCs, China has suffered from extremely high and
47 continuously increasing O₃ pollution from 2013 to 2019 with the peak season daily
48 maximum 8-hour average (MDA8) O₃ concentration over 95 μg m⁻³. The rising trend
49 has been reversed since 2020, along with the national annual NO_x and non-methane
50 VOCs (NMVOCs) emissions reduced by 28.3 % and 3.8 %, respectively during
51 2013–2020 (Zheng et al., 2018; Xiao et al., 2022; Liu et al., 2023a; Wang et al., 2023).
52 However, current O₃ concentration over China is still much higher than the global air
53 quality guidelines (60 μg m⁻³ for the averaged peak season MDA8 O₃, WHO, 2021).
54 This presents a great challenge for the country to meet the criteria for public health
55 welfare in the future (Feng et al., 2023; Jiang et al., 2023).

56 In addition to the anthropogenic driver, studies also addressed the roles of
57 meteorological factors, biogenic VOCs (BVOCs) emissions and transboundary
58 transport of pollutants on O₃ enhancement in China (Monks et al., 2015; Lu et al.,
59 2019; Cao et al., 2022; Wang et al., 2022; Weng et al., 2022; Jiang et al., 2023).
60 Meteorological factors, including temperature, humidity, wind, etc., influence the
61 chemical reactions associated with O₃ production and elimination, and the
62 transportation of O₃ precursors (Gong and Liao, 2019). The changed meteorology was
63 estimated to enhance the summer MDA8 O₃ concentration by 1.4 ppb yr⁻¹ during
64 2013–2019 in the North China Plain (NCP), nearly half of the overall O₃ growth of
65 3.3 ppb yr⁻¹ (Li et al., 2020a). BVOCs refer to VOCs emitted from terrestrial
66 ecosystems and possess high reactivity in atmospheric chemical processes, mainly
67 including isoprene, monoterpenes and sesquiterpene (Wu et al., 2020a). Cao et al.
68 (2022) reported that BVOCs emissions in summer 2018 enhanced 8.6 ppb MDA8 O₃
69 averaged over China with the highest contribution over 30 ppb in southern China.

70 Moreover, O₃ and its precursors could be transported over long distance, and
71 transboundary foreign anthropogenic emissions were estimated to contribute 2–11
72 ppb to near surface O₃ in China (Ni et al., 2018; Han et al., 2019).

73 In the context of future global change, substantial but uncertain changes will
74 occur in economy, climate and land cover. According to the Sixth Assessment Report
75 of Intergovernmental Panel on Climate Change (IPCC AR6 report), the global surface
76 temperature will increase 0.2–3.7 °C till 2100 under different scenarios compared to
77 2015 (IPCC, 2021, 2022). As a result, unfavorable meteorological extremes, such as
78 high temperature extremes and ecological drought events, will be more frequent and
79 intense (Hong et al., 2019; Porter and Heald, 2019; IPCC, 2021), leading to the
80 deterioration of air quality named as climate penalty. To conquer the climate change
81 and resulting air quality deterioration, a series of measures will be implemented, such
82 as accelerating the transition to clean energy, upgrading industrial production
83 technologies and strengthening pollution control measures. Attributable to these
84 changes, annual mean surface O₃ in East Asia was projected to change by –13.9–6.1
85 ppb till 2100 compared to 2015 (IPCC, 2021). However, limited by the coarse
86 resolution of earth system model and the lack of consideration of the regional
87 measures for reducing air pollution and carbon emissions, global estimation is
88 insufficient for understanding how O₃ pollution in China will respond to the complex
89 future change.

90 There have been some studies on how the above-mentioned changes will affect
91 future O₃ level in China. Hong et al. (2019) reported that the 1-hour maximum O₃ in
92 April to September will be enhanced by 2–8 ppb within large areas of China under
93 RCP4.5 (representative concentration pathways 4.5, van Vuuren et al., 2011) scenario
94 from the 2010s to 2050s. Under high-forcing scenarios, Li et al. (2023) projected the
95 climate-driven O₃ concentration in the 2100s and found that O₃ concentration in
96 southeast China would increase 5–20 % compared to the 2020s by a machine learning
97 method. A warming climate should enhance the O₃ level, given the increasing

98 frequency of atmospheric stagnation and heat waves (Hong et al., 2019; Wang et al.,
99 2022; Gao et al., 2023; Li et al., 2023). The effect of anthropogenic emission change
100 on China's O₃ level has been estimated by studies under different scenarios. Zhu and
101 Liao (2016) applied global emission estimates under RCPs, and found that the
102 maximum growth of annual mean O₃ would be 6–12 ppb during 2000–2050 under
103 different scenarios. Using the Dynamic Projection model for Emissions in China
104 (DPEC) that better includes local information of energy transition and emission
105 controls (Cheng et al., 2021b), Xu et al. (2022) reported that the joint impact of
106 climate change and emission reduction would reduce the annual MDA8 O₃
107 concentration to 63.0 µg m⁻³ under ambitious scenario of carbon neutrality. Biogenic
108 emission change is another factor influencing future O₃ (Chen et al., 2009; Andersson
109 and Engardt, 2010; Harper and Unger, 2018; Wang et al., 2020). Liu et al. (2019)
110 predicted a 24 % growth of BVOCs emissions driven by climate change under
111 RCP8.5 from 2015 to the 2050s, resulting in a variation of daily 1-h maximum O₃
112 concentration ranging from -10.0 to 19.7 ppb across different regions in China.

113 Limitations exist in current studies, which prevent comprehensive assessment and
114 understanding of the joint impacts of future changes of multiple factors on China's O₃
115 pollution. Firstly, the above estimations mainly focused on the influence of future
116 changes on summertime or annual average O₃ concentration. As China's O₃ pollution
117 has been reported to spread into spring and fall, it is of great importance to separate
118 the impacts on warm (April to September, the six months with heaviest O₃ pollution
119 for most part of China, Liu et al., 2023a) and non-warm season O₃ (October to March),
120 considering the diverse air pollution sources and O₃ formation sensitivity to
121 precursors for different seasons (Li et al., 2021; Wang et al., 2023). Recent studies
122 have suggested diverse effects of future emission change on O₃ evolution for
123 difference seasons in China (Hou et al. 2023; Liu et al. 2023b). In addition, the rising
124 frequency of extreme weathers and declining anthropogenic emissions will further
125 influence the possibility of extreme O₃ events, which has been scarcely discussed.

126 Secondly, to restrain global warming, China has made a national commitment to
127 achieving “carbon neutrality” by 2060 (Shi et al., 2021), and accordingly launched a
128 series of energy and climate action plans to reduce greenhouse gas emissions. These
129 actions will also cause substantial reductions in air pollutant emissions, but have not
130 been fully included in existing predictions of global emissions (Tong et al., 2020;
131 Cheng et al., 2021b). Large bias will then be caused in the simulation of
132 anthropogenic-induced future changes of air quality, with a less realistic estimate of
133 local emission path (Cheng et al., 2021a). Due to probably faster decline of emissions
134 in China but slower in surrounding countries in the future, the contributions of
135 transboundary emissions on China’s O₃ can be greatly changed and has not yet been
136 fully considered (Hou et al., 2023). Thirdly, BVOCs emissions will not only be
137 affected by meteorological factors but also by land use and land cover change
138 (Penuelas and Staudt, 2010; Szogs et al., 2017; Wang et al., 2021a). Future land
139 management will change due to socio-economic development and necessary actions
140 as climate change response, and the changed shares of forest, cropland and grassland
141 will alter the magnitude and distribution of BVOCs emissions and thereby affect O₃
142 concentration (Hurtt et al., 2020; Liao et al., 2020; Liu et al., 2022). Finally, the
143 existing evaluations were conducted separately for individual influencing factors, with
144 diverse methods and data. The interactions between different factors were seldom
145 included in existing analyses, and the relative contributions of multiple factors were
146 difficult to be evaluated or compared. Relevant studies have been conducted in
147 developed countries (Gonzalez-Abraham et al., 2015), and are still lack in China.

148 In this study, we evaluate the complex influence of future changes of multiple
149 factors on surface O₃ concentration in China within a uniform framework. The
150 evaluation is conducted from the perspectives of seasonal, regional and extreme
151 events of O₃ pollution. Four factors are included in the analyses, i.e., meteorological
152 conditions, local anthropogenic emissions, BVOCs emissions, and anthropogenic
153 emissions from surrounding foreign countries. The analyses are conducted based on a

154 series of sensitivity experiments in numerical modelling of future air quality, and
155 up-to-date input data from multiple sources are utilized in the model (see details in
156 next section). We provide a comprehensive perspective on the spatiotemporal change
157 of China's O₃ pollution till the 2060s, under a moderate way SSP2 of Shared
158 Socioeconomic Pathways (SSPs, Riahi et al., 2017) and a midrange mitigation
159 scenario RCP4.5, a scenario at the middle of the socio-economic developing way with
160 radiative forcing at 4.5 W m⁻² nominally by 2100 (Meinshausen et al., 2020). The
161 outcomes highlight the regional and seasonal heterogeneity of O₃ pollution risks
162 driven by complex future change of multiple factors, and support strategy design of
163 O₃ pollution alleviation with specific principles, targets and action pathways.

164 **2 Data and Methods**

165 **2.1 Main framework and research domain**

166 The simulation framework incorporates the Weather Research and Forecasting
167 model (WRF, version 3.7.1) to generate hourly meteorological fields, the Model
168 of Emissions of Gases and Aerosols from Nature (MEGAN, version 2.1) to calculate
169 gridded BVOCs emissions, and the Community Multiscale Air Quality model
170 (CMAQ, version 5.2) to simulate O₃ concentration. BVOCs emission calculations and
171 air quality simulations are driven by meteorological fields of 2018–2022 (the 2020s,
172 representing the current situation) and 2058–2062 (the 2060s, representing the future
173 situation). All simulation results are averaged over a period of five years to mitigate
174 the influence of interannual variability of meteorology. The modelling domain, same
175 for WRF, MEGAN and CMAQ, covers East Asia, most areas of South Asia and
176 Central Asia, and part of Southeast Asia and North Asia (Figure 1). It applies the
177 Lambert Conformal Conic projection centered at (110° E, 34° N), and the horizontal
178 resolution is 27 km×27 km, with 303×203 grids. The target area, Chinese mainland,
179 includes 31 provincial-level administrative regions (excluding Hong Kong, Macao
180 and Taiwan). Eight geographical regions are defined, and locations of the three

181 regions with dense population and relatively heavy air pollution are also shown in
182 Figure 1, namely BTH (Beijing-Tianjin-Hebei), YRD (Yangtze River Delta) and PRD
183 (Pearl River Delta).

184 **2.2 Data sources and processing methods**

185 We use the bias-corrected RCP4.5 output of the National Center for Atmospheric
186 Research's Community Earth System Model (NCAR CESM) as initial and boundary
187 conditions for WRF (Monaghan et al., 2014). A ten-year dynamic downscaling
188 simulation for 2018–2022 and 2058–2062 is conducted. Note we do not utilize the
189 real-time reanalysis data to drive the simulation of the 2020s, in order to minimize the
190 systematic error between the simulation driven by real meteorological conditions (for
191 current simulations) and climate projection (for future simulations),

192 The BVOCs emissions are basically determined by meteorology and vegetation.
193 The meteorological conditions are supplied by WRF. The vegetation data, including
194 leaf area index (LAI), plant functional types (PFTs) and emission factors (EFs) of
195 each PFT, are determined for 2020 and 2060. Gridded LAI data for 2020 are obtained
196 from Global Land Surface Satellite product (Liang et al., 2021), and those for 2060
197 under SSP2-45 scenario are downscaled from the daily CESM2 output of Coupled
198 Model Intercomparison Project Phase 6 (CMIP6). PFTs data for 2020 are derived
199 from MCD12C1 product of Moderate-Resolution Imaging Spectroradiometer
200 (MODIS) dataset and mapped to the 16 types required for MEGAN following Liao et
201 al. (2020). The PFTs data for 2060 in China are obtained from Liao et al. (2020)
202 under SSP2-45 scenario, with other regions maintaining those of 2020. EFs for each
203 PFT are taken from Guenther et al. (2012).

204 Anthropogenic emissions for Chinese mainland are obtained from the
205 Multi-resolution Emission Inventory for China (MEIC,
206 http://meicmodel.org.cn/?page_id=560) for 2020, and DPEC version 1.1 under
207 SSP2-45 incorporating the best available end-of-pipe pollution control technologies
208 for 2060. The annual total eEmissions by country/region outside Chinese mainland

209 are obtained from CMIP6 dataset under SSP2-45 scenario (O'Neill et al., 2016;
210 Gidden et al., 2019), and These emissions are downscaled into gridded monthly
211 data for CMAQ simulation, based on the spatial and temporal distributions of
212 ~~emissions outside Chinese mainland are assumed the same as those~~ in MIX Asian
213 emission inventory (Li et al., 2017). The speciation profiles of NMVOCs are taken
214 from MIX as well. Supplementary Figure S1 shows the emissions of two main
215 precursors of O₃ by year and region. The NO_x and NMVOCs emissions for Chinese
216 mainland were estimated to decline 58 % and 51 % from 2020 to 2060, respectively,
217 much faster than those of surrounding areas within the modelling domain (8 % and
218 14 % respectively). In particular, the NO_x emissions would decline 57–62 % for the
219 three developed regions BTH, YRD and PRD, while the reductions of anthropogenic
220 NMVOCs would vary a lot among regions (36 %, 49 % and 60 % for BTH, YRD and
221 PRD, respectively).

222 Carbon Bond 2005 (CB05, Yarwood et al., 2005) is adopted as the gas-phase
223 chemical mechanism and the sixth-generation CMAQ aerosol module AERO6 (Appel
224 et al., 2013) as aerosol chemistry mechanism. The initial and boundary conditions are
225 set by default clean air conditions in CMAQ, and the first 10 days for each year are
226 determined as the spin-up period to minimize the effects of initial and boundary
227 conditions.

228 **2.3 Simulation cases**

229 Six cases of CMAQ simulations are conducted to investigate the impacts of
230 future change of the four factors on O₃ concentration in China (Table 1). Cases 1 and
231 2 represent the current (2020s) and future (2060s) baseline, respectively, and the
232 difference between them indicates the joint effect of the future changes of multiple
233 factors. Each of Cases 3–6 applies the prediction for 2060s for one specific factor but
234 keeps the remaining factors at current condition (2020s). Thus, the difference between
235 each of those four cases and Case 1 indicates the impact of individual factor,
236 including meteorological conditions (Case 3), domestic anthropogenic emissions

237 (Case 4), BVOCs emissions (Case 5) and anthropogenic emissions of surrounding
238 countries (countries other than Chinese mainland within the modeling domain, Case
239 6). Surrounding areas refer to areas within the modelling domain but excluding
240 Chinese mainland. Each case contains a five-year (2018–2022 or 2058–2062)
241 WRF-MEGAN-CMAQ simulation driven by the varying meteorological conditions
242 for individual years, and the five-year average of simulated O₃ concentrations is
243 adopted for further analyses.

244 **2.4 Model performance**

245 To evaluate the model performance, we conduct a comparative analysis between
246 simulations and observations for meteorological factors and O₃ concentrations, as
247 well as an intercomparison for BVOCs estimates between different studies.

248 We first examine the capability of downscaled CESM climate projections in
249 capturing the meteorological conditions of the 2020s. We applied the meteorological
250 data from the National Climate Data Center (NCDC, archived at
251 <https://soft.net/air>) in 2020, and the statistical metrics are presented in
252 Supplementary Table S1. The modeled temperature at 2 m (T2) is in good
253 spatiotemporal agreement with the observations, with the correlation coefficient (R)
254 of 0.96 and index of agreement (IOA) of 0.98. The relative humidity (RH) is also well
255 predicted with R and IOA at 0.78 and 0.88, respectively. The model shows an
256 overestimation on the wind speed by 1.41 m s⁻¹, which is also reported by Hu et al.,
257 (2022). The correlation coefficients of wind speed and direction are higher than 0.5.
258 Overall, the modeled meteorological fields have basically captured the conditions in
259 China and are appropriate for subsequent MEGAN and CMAQ simulations.

260 For BVOCs emissions, we compare our estimates for the 2020s with previous
261 studies, as summarized in Supplementary Table S2. The total BVOCs, isoprene and
262 terpenes emissions in this study are estimated at 33.55, 21.08 and 3.30 Tg yr⁻¹,
263 respectively, and are comparable to other studies. In particular, our estimate is larger
264 than others except for Li et al. (2020b) for isoprene, while smaller than others except

265 for Wu et al. (2020a) for terpenes. The differences between studies might result from
266 the diverse strategies of mapping PFTs from the original satellite products and the
267 difference between downscaled climate conditions and the real meteorological fields.

268 We apply the observed MDA8 O₃ concentration data from the national network
269 of China Ministry of Ecology and Environment (archived at <https://quotsoft.net/air>) to
270 evaluate CMAQ performance. As shown in Supplementary Figure S2, the simulation
271 could capture the spatiotemporal distribution of surface MDA8 O₃ concentration for
272 the whole country and specific O₃ pollution hot spots, e.g., BTH and eastern Sichuan
273 province with their surrounding areas. The statistical metrics of the comparisons
274 between the simulated and observed monthly average MDA8 O₃ concentration of
275 2020s are summarize in Supplementary Table S1. The normalized mean biases (NMB)
276 are calculated at 14.12 % and 10.90 % for warm and non-warm season, and R values
277 at 0.71 and 0.32, respectively. Even with a slight overestimation, the reliability of our
278 simulation is comparable to most previous studies in China, with a better performance
279 in the warm season (Hu et al., 2016; Lu et al., 2019; Gao et al., 2020; Yang and Zhao,
280 2023).

281 ~~In addition, we~~ We evaluate the interannual variability within each of the
282 five-year simulations, based on using the coefficient of variation (CV), the ratio of
283 standard deviation and to mean of the simulated O₃ concentrations. As is shown in
284 Supplementary Table S3, the CVs are generally below 5 % in most cases, indicating
285 relatively small interannual variability that in the simulated O₃ concentrations
286 exhibited simulation relatively low interannual variability. This suggests results thus
287 justify the representativeness of the five-year averages for present and future
288 scenarios. s that the concentrations are stable and closely centered around the mean,
289 with minimal fluctuation across the five year simulations.

290 **3 Results and Discussions**

291 **3.1 Future change of meteorology and BVOCs emissions**

292 The downscaled changes in the meteorological factors from the 2020s to 2060s
293 (SSP2-45 scenario) are shown in Figure 2, including temperature, RH and wind speed
294 (WS). The changes are analyzed separately for April–September (warm season) and
295 October–March (non-warm season). For the warm season, daily maximum
296 temperature at 2 m (T-max) will increase across China with an average change of
297 1.0 °C, and the minimum and maximum changes are found in Tibetan Plateau at 0.1 °C
298 and in Heilongjiang province at 2.1 °C, respectively. The RH will decrease slightly by
299 –0.6 % for the whole country, with the changes for most areas within the range
300 between –3 % and 0 % except for some areas of Northwestern China, Southwestern
301 China, and Tibetan Plateau (see the region definitions in Figure 1). The growing
302 T-max and declining RH will enhance the photochemical production of O₃ and
303 BVOCs emissions. For the non-warm season, the national average growth of T-max
304 will be smaller at 0.2 °C and some areas in Northeastern, Northern and Eastern China
305 will even experience a decline ranging from –1.8 to 0 °C. The RH will change
306 diversely across the country, ranging from –6.0 to 6.3 %. Very limited change in WS
307 will occur, ranging from –0.1 to 0.2 m s⁻¹ in most areas of the country. Generally, the
308 decreasing wind speed in future East Asia could be attributed to weakened
309 atmospheric circulation (Coumou et al., 2018; Deng et al., 2021). The increasing wind
310 speed in non-warm season might result from the temperature and pressure gradients
311 between the land and adjacent oceans (Yao et al., 2019; Wu et al., 2020b). The spatial
312 distribution of downscaled future meteorological field changes is generally in
313 agreement with those predicted by Hong et al. (2019) and Hu et al. (2022). Some
314 discrepancies in temperature and wind speed change of non-warm season between
315 studies result from the different choices of base year and parameterization schemes of
316 WRF.

317 Table 2 shows China’s BVOCs emissions of the 2020s and 2060s (SSP2-45
318 scenario) estimated with MEGAN, as well as the BVOCs emission intensity
319 (emissions per unit area) for the three developed regions. The emissions will increase

320 from 33.6 Tg yr⁻¹ for the 2020s to 43.4 Tg yr⁻¹ for the 2060s. The growth rates in
321 BTH, YRD and PRD are predicted to be ~~22~~21.4 %, 23.9 % and 23.0 %, respectively,
322 smaller than that for the whole country (29.2 %). The spatial distributions of BVOCs
323 emissions for the 2020s and the changes from the 2020s to 2060s, are shown in
324 Supplementary Figure S3. Areas all over China will experience the growth of BVOCs
325 emissions, and it will be more prominent in areas with high vegetation coverage (e.g.,
326 Southern and Southwestern China) rather than urban areas. The growth of BVOCs
327 emissions will enhance the contribution of natural sources to O₃ formation, especially
328 along with declining anthropogenic emissions in the future (Penuelas and Llusia, 2003;
329 Riahi et al., 2017; Gao et al., 2022).

330 **3.2 Response of surface O₃ concentration to combined future changes**

331 Figure 3 illustrates the spatial distributions of MDA8 O₃ concentrations for the
332 warm and non-warm seasons of the 2020s and 2060s (SSP2-45 scenario), as well as
333 the differences between the two periods. Briefly, future changes of the four factors
334 under SSP2-45 are estimated to jointly reduce MDA8 O₃ by 7.7 and 1.1 ppb in the
335 warm and non-warm season, respectively, while the O₃ responses to future changes
336 will differ by region.

337 In the warm season of the 2020s (Figure 3a), the nationwide average MDA8 O₃
338 concentration is simulated at 57.3 ppb, and those of BTH, YRD and PRD are 73.7,
339 68.7 and 52.3 ppb, respectively. Hot spots of O₃ pollution, with average MDA8 O₃
340 over 75 ppb, are mainly located in Northern China and Sichuan province. The pattern
341 is predicted to persist into the 2060s (Figure 3b), with a decline in both the severity
342 and size of highly polluted regions. The nationwide MDA8 O₃ concentration will
343 decline 13.4 % to 49.6 ppb, and that in most areas of China will be within the range of
344 37.5–67.5 ppb. The highest concentration will be lower than 75 ppb for the two
345 hotspots of Northern China and Sichuan. BTH will remain as the most O₃-polluted
346 area in warm season, with the O₃ concentration at 63.9 ppb (13.3 % smaller than the
347 2020s), while that of YRD and PRD will decrease to 53.9 (21.5 %) and 39.8 ppb

348 (23.9 %), respectively. O₃ concentration in the developed regions will decline faster
349 than or roughly the same as that for the whole country. The reductions in MDA8 O₃
350 from 2020s to 2060s will be 10–20 ppb for Northern, Eastern, Central and Southern
351 China and 0–10 ppb for Northeastern and Northwestern China as well as the Tibetan
352 Plateau (Figure 3c). Notably, some areas in Sichuan are expected to experience a
353 substantial decline of MDA8 O₃ over 20 ppb.

354 O₃ concentration of the non-warm season is simulated to be much lower than that
355 of the warm season. The 2020s average MDA8 O₃ is 48.4 ppb, ranging from 30.0 to
356 67.5 ppb in most areas of China (Figure 3d). Different from the warm season in which
357 highest concentration is found for Northern China and Sichuan, the Southern and
358 Southwestern parts of China suffer the highest O₃ level for the non-warm season. A
359 general west-to-east and south-to-north gradient is found for MDA8 O₃, with the
360 lowest concentration found in Northern and Northeastern China. The concentrations
361 in BTH and YRD are simulated at 33.8 and 45.1 ppb, respectively, much lower than
362 that of PRD (58.9 ppb). Relatively high temperature during even the non-warm season
363 is expected to expand the O₃ pollution period in Southern China. Resulting from
364 complex change of multiple factors, the national average MDA8 O₃ concentration in
365 the non-warm season of 2060s will decrease slightly to 47.3 ppb under SSP2-45, and
366 that in most regions will be within the range of 37.5–52.5 ppb except for some areas
367 in Northeastern China and Tibetan Plateau (Figure 3e). The MDA8 O₃ concentrations
368 of the three developed regions will become closer at 39.3, 48.4 and 51.6 ppb for BTH,
369 YRD and PRD, respectively. As illustrated in Figure 3f, MDA8 O₃ is predicted to
370 increase in BTH and YRD and the surrounding areas, with the growth mostly ranging
371 0–15 ppb. In other areas (especially in Southern China), the concentration will
372 decrease in the non-warm season by –15 to –5 ppb. As a result of the increased O₃ in
373 the less polluted Eastern and Northern China and decreased O₃ in the more polluted
374 Southwestern and Southern parts, the 2060s regional disparity in the non-warm season
375 O₃ pollution will get smaller compared to the 2020s (Figure 3d and 3e).

376 To further explore the temporal pattern of O₃ level in the future, we compare the
377 monthly average MDA8 O₃ in the 2020s and 2060s under SSP2-45 for the whole
378 country and three developed regions (Figure 4 and Supplementary Figure S4). For the
379 whole country (Figure 4a), the changes of monthly average MDA8 O₃ from 2020s to
380 2060s are estimated to range from -3.2 to -10.7 ppb in the warm season but less
381 prominent in the non-warm season (from -2.7 to 0.9 ppb). Along with the more
382 reduction in summertime (June, July and August), in particular, the periods with the
383 highest O₃ concentration will expand into spring (March) and fall (October), as
384 presented in Supplementary Figure S4. For the three regions, a greater decline in O₃
385 concentration is found in the warm season while a smaller or even a growth is found
386 in the non-warm season. For BTH (Figure 4b), the monthly MDA8 O₃ concentrations
387 range between 24.7 and 88.4 ppb in the 2020s with a clear difference between the
388 warm and non-warm season. This pattern will remain in the 2060s with smaller
389 difference between months (30.6–70.2 ppb). The temporal change pattern of YRD is
390 similar to that in BTH, with decline in the warm season and growth in the non-warm
391 season (Figure 4c). The shift of O₃ pollution from the warm towards the non-warm
392 season is more prominent in the PRD, the only region where O₃ concentration of all
393 the months in 2060s is predicted to decline (Figure 4d). Different from BTH and YRD,
394 as mentioned above, higher O₃ concentrations during spring and autumn and lower in
395 summer (due to the abundant summertime precipitation and high humidity) are found
396 for PRD in the 2020s (Gao et al., 2020; Han et al., 2020). With great O₃ decline in the
397 warm season, the periods experiencing peak O₃ pollution are predicted in the
398 non-warm season of the 2060s, predominantly between October and March
399 (Supplementary Figure S4).

400 **3.3 Identifying surface O₃ response to individual factors**

401 **3.3.1 Local anthropogenic emission change**

402 Figure 5 shows the influences of changes of each individual factors (local

403 anthropogenic emissions, meteorological conditions, BVOCs emissions, and
404 anthropogenic emissions from surrounding countries) on the warm and non-warm
405 season O₃ concentrations. Out of the four, the change of local anthropogenic
406 emissions is predicted to be the most influential factor, resulting in a national average
407 decline of 7.2 and 0.8 ppb for the warm and non-warm season, respectively (Figure 5a
408 and 5e). In the warm season, the emission reduction will play a positive role in
409 reducing O₃ pollution in most areas of China, and the decrease will exceed 10 ppb
410 across Northern, Eastern, Central, Southern and part of Southwestern China. In the
411 non-warm season, emission reduction will have contrasting effects on MDA8 O₃
412 levels in the north and south part of China, enhancing MDA8 O₃ by 0–15 ppb for the
413 former while restraining it by 0–10 ppb for the latter. Especially, the emission
414 reduction is predicted to elevate the O₃ concentration by 5.9 and 4.0 ppb for BTH and
415 YRD respectively.

416 Supplementary Figure S5 shows the relative emission reductions from 2020s to
417 2060s by region. Under SSP2-45 scenario, the reductions of NO_x and VOCs
418 emissions will range from 35.6 % to 63.6 % for different regions, and VOCs emission
419 reduction will be less than that of NO_x except for PRD. As the NO_x-limited regime for
420 O₃ formation (i.e., O₃ is more sensitive to NO_x emission change) occurs more
421 frequently in the warm season while the VOC-limited regime more in the non-warm
422 season, the larger decline of NO_x emissions than VOCs should be more effective in
423 restraining the warm season O₃ pollution but has less benefit or even negative effect
424 in the non-warm season (Sillman and He, 2002). Wintertime of NCP and YRD have
425 been reported under the VOC-limited regime and the excessive NO_x emissions play
426 an important role in removing O₃ by titration effect (Jin and Holloway, 2015; Li et al.,
427 2021; Wang et al., 2021b). This may explain the MDA8 O₃ increase during the
428 non-warm season with insufficient reduction of VOCs (35.6 % and 49.5 %) but sharp
429 reduction of NO_x of 53.4 % and 60.3 % for NCP and YRD, respectively. Similarly,
430 Hou et al. (2023) and Liu et al. (2023b) also predicted a growth of O₃ concentration in

431 non-warm season over BTH and YRD under a net-zero carbon emission scenario,
432 resulting from a weakened titration effect. Supplementary Figure S6 shows the
433 monthly variation of O₃ and odd oxygen (O_x, O_x=O₃+NO₂, representing the real
434 photochemical production potential of O₃ considering the titration effect) in the 2020s
435 and 2060s. It should be noted that the growth of O₃ in the non-warm season in 2060s
436 for BTH and YRD will be accompanied by minimal change of O_x, while the declines
437 of O₃ and O_x will appear simultaneously in the warm season for the three regions and
438 in non-warm season for PRD. This indicates that the growth of non-warm season O₃
439 in BTH and YRD should result partly from NO_x reduction and thereby weakened NO
440 titration, as titration is a key pathway of O₃ loss when the chemical reactivity is
441 relatively low in winter (Gao et al., 2013; Akimoto and Tanimoto, 2022). The
442 differentiated O₃ responses to precursor reduction between YRD and PRD have also
443 been detected during the COVID-19 breakout period. With the O₃ isopleth plots,
444 Wang et al. (2021b) illustrated that 40–60 % reduction of NO_x and VOCs enhanced
445 the O₃ formation in YRD under the VOC-limited regime but suppressed O₃ in PRD
446 under the transitional regime (a regime between NO_x- and VOC-limited). Therefore,
447 VOCs emission controls should be better addressed for O₃ pollution alleviation when
448 it expands to non-warm season in the future.

449 3.3.2 Meteorological condition change

450 As shown in Figure 5b and 5f, the influence of meteorological change exhibits
451 different patterns for the warm and non-warm season.—
452 In the warm season, meteorological change due to global warming will play a positive
453 role on O₃ formation in most of China, with the enhancement within 0–4 ppb, but it
454 will reduce the O₃ level in remote areas like Tibetan Plateau. The national average
455 growth will be 0.3 ppb and that for YRD, PRD and BTH will be 1.9, 0.7, and 0.3 ppb,
456 respectively. The response of O₃ to meteorological change is associated with some
457 specific variables (Hong et al., 2019). For example, the great enhancement of O₃ in
458 YRD might be attributable to a hotter, dryer and more stable atmosphere with growth

459 of T-max (over 0.6 °C) and decline of RH and WS (Figure 2). The result is similar to
460 Hong et al. (2019), which reported a change of 2–8 ppb of daily 1-hour maximum O₃
461 concentration for the peak season from the 2010s to 2050s under RCP4.5. In addition,
462 the declining O₃ in Tibetan Plateau and the surrounding areas might result partly from
463 the weakened long-range transport of peroxyacetyl nitrate (PAN, the principal NO_x
464 reservoir) from the polluted areas (Fischer et al., 2014). Driven by the elevated
465 temperature, PAN from relatively polluted regions will undergo stronger thermal
466 decomposition locally, thus fail to be transported far away to the remote regions to
467 promote O₃ formation (Liu et al., 2013; Lu et al., 2019).

468 The influence of meteorological change on O₃ production is predicted to be much
469 smaller for the non-warm season, with the magnitude within ±1 ppb in most areas and
470 nationwide average at -0.2 ppb. In the three developed regions, the changes are
471 predicted to range from -0.4 to 0.3 ppb, with little regional difference. The limited
472 influence might be attributable to the modest change in temperature and RH in the
473 non-warm season.

474 **3.3.3 BVOCs and surrounding anthropogenic emission change**

475 Compared to domestic emissions, change of BVOCs emissions and
476 anthropogenic emissions from surrounding countries will have a less influence (within
477 ±3 ppb) on surface O₃ concentration in China. BVOCs change tends to enhance O₃
478 while foreign emission change tends to restrain it in most areas (Figure 75).

479 The growing BVOCs emissions due to vegetation and climate change is estimated
480 to enhance O₃ concentration by 0–3 ppb in the most areas of China, with a larger
481 influence of 0.6 ppb in the warm season than that of 0.3 ppb in the non-warm season
482 across the country (Figure 5c and 5g). In the warm season, relatively large growth of
483 O₃ concentration will occur in BTH at 2.1 ppb, and those of YRD and PRD will be
484 1.5 and 1.0 ppb, respectively. The abundant NO_x emissions in BTH are expected to
485 result in a larger O₃ concentration response to BVOCs emission change than YRD
486 and PRD, even the BVOCs emission change of BTH will be smaller than the other

487 two regions (Table 2). The result is in agreement with other numerical simulation
488 experiments. Liu et al. (2019) reported a prominent O₃ enhancement even with a low
489 BVOCs emission rate under RCP8.5, in a NO_x-abundant environment. In the remote
490 areas like Tibetan Plateau and part of Northeastern China, the increased BVOCs will
491 remove O₃ due to the isoprene ozonolysis in low-NO_x environment (Hollaway et al.,
492 2017; Zhu et al., 2022). In general, regions with higher O₃ pollution levels and NO_x
493 emissions will suffer more risk of O₃ growing from rising BVOCs emissions in the
494 future.

495 Most areas of China will benefit from the foreign emission change in terms of O₃
496 pollution alleviation (Figure 5d and 5h). An exception is Tibetan Plateau and its
497 surrounding areas, which will be affected by the elevated emissions of NO_x and VOCs
498 from South Asia under SSP2-45. Limited by the range of pollutant transport, greater
499 impacts will be found for coastal and border areas and less for inland areas (Ni et al.,
500 2018). Larger O₃ changes in the three developed regions are predicted than that of the
501 whole country, benefitting from the precursor emission reduction in East Asia and
502 Southeast Asia.

503 **3.4 The relationship between the joint and separate effects of multiple factors**

504 Figure 6 summarizes the contributions of individual factors to the total O₃ change
505 by region and season. Due to the nonlinear response of O₃ to multi-factor changes, the
506 aggregated contribution of the four factors does not equal to the joint contribution (i.e.,
507 there exist gaps between the difference of the 2020s and 2060s and the aggregated
508 contribution of four factors).

509 The varying domestic anthropogenic emissions are predicted to dominate the
510 change of the future O₃, with a relative contribution ranging from 75 % to 117 % for
511 different regions and seasons. The relative contributions of the other three factors are
512 estimated to be limited within ±25 % at national and regional level. Among different
513 regions, YRD will be more affected by climate change with the contribution of -13 %
514 and -12 % for the warm and non-warm season, respectively, far greater than that of

515 BTH and PRD (−6 % to 0 %). BTH will be more affected by BVOCs emission
516 change than other regions in the warm season (−21 %), while YRD and PRD will be
517 more affected in the non-warm season with the relative contributions of 17 % and
518 −20 %, respectively. Little regional difference is found for the relative contributions
519 of foreign emission change.

520 To better understand the regional and seasonal differences of the relative
521 contributions of future changes to O₃ concentration, we examine the nonlinear
522 response of O₃ to precursor change in the three developed regions. We follow Chen et
523 al. (2021) and Schroeder et al. (2017), and conduct a fit of lognormal distribution for
524 the relationship of modeled hourly O₃ and NO₂ concentrations, as shown in Figure 7.
525 The data points on the left of the turning point of fitted curve suggest a NO_x-limited
526 regime while on the right a VOC-limited regime, and data points around the turning
527 point are under transitional regime.

528 The O₃-NO₂ relationship from the 2020s to 2060s will be mostly influenced by
529 the changing domestic anthropogenic emissions, indicated by the close distributions
530 of data points and fitted curves between “EMIS” and “2060s” in Figure 7. In the
531 warm season, the future O₃-NO₂ relations in BTH and YRD are predicted to change
532 greatly from a highly O₃ polluted situation with moderate NO₂ concentration to a
533 situation with a relatively low level of NO₂ (mostly under 10 ppb) and a moderate
534 level of O₃ (under 60 ppb). A weak VOC-limited regime appeared for the whole BTH
535 in 2020s, ~~and it is consistent with recent observation-based analysis (Chen et al. 2023;~~
536 ~~Kong et al. 2024).~~ ~~and~~ ~~†~~ There is big diversity within the region, including a dense area
537 with strong VOC-limited regime and other areas with transitional or NO_x-limited
538 regime (Figure 7a). Represented by the moving of most points from the right of the
539 turning point to near or left of the turning point, the NO_x-limited and transitional
540 regimes will dominate BTH in the 2060s. Compared to 2020s, the data points of
541 2060s are more closely distributed, indicating a reduced diversity of O₃ formation
542 regime in the region. For YRD, most areas were under transitional or weak

543 VOC-limited regime in the 2020s with limited diversity within the region, and the
544 situation in 2060s will be similar to that of BTH (Figure 7a and 7b). The shift from
545 weak VOC-limited regime in 2020s to transitional or NO_x-limited regime in 2060s for
546 BTH and YRD implies the influence of emission reduction on altering the sensitivity
547 of O₃ formation to precursors. Most areas of PRD in the 2020s are under transitional
548 or NO_x-limited regimes, and the regime will transfer to a strong NO_x-limited one in
549 2060s, with an almost positive correlation between NO₂ and O₃ in a low-NO₂
550 environment (Figure 7c). In the non-warm season, O₃ and NO₂ will remain negatively
551 correlated for BTH and YRD till the 2060s, which suggests a persistent VOC-limited
552 regime and explains the O₃ concentration growth along with substantial precursor
553 emission reductions. The turning points are simulated at extremely low NO₂
554 concentrations of 2.0 and 1.2 ppb for BTH and YRD, respectively (Figure 7d and 7e).
555 A big challenge still exists on effective emission controls to reduce the O₃
556 concentration in the non-warm season for the two regions. Differently, the O₃
557 formation sensitivity in most of PRD will shift from transitional regime towards a
558 more NO_x-limited situation (Figure 7f). A simple comparison with the O₃ evolution
559 and its precursor emission changes in developed country provided more policy
560 implication. According to Chen et al. (2021) and the US Environmental Protection
561 Agency, the northeastern US ~~underwent~~ experienced rapid cross of the turning point of
562 O₃ formation sensitivity during 1990s–2010s, with approximately 60 % reductions in
563 both anthropogenic NO_x and VOCs emissions. However, In BTH, the emissions
564 declines are predicted to decline be 57 % and 36 % for NO_x and NMVOCs during
565 2020s–2060s for BTH under SSP2-45 scenario. To accelerate the shift in the O₃
566 chemical regime for BTH, Therefore, more ambitious reductions in NMVOCs will be
567 necessary (—potentially ideally —even double the current projected efforts abatement
568 under SSP2-45), to accelerate the shift in the O₃ chemical regime for BTH.:

569 The fitted curves of other three factors are similar to those of the 2020s, and the
570 change of these factors will make little difference on NO₂ concentration but will result

571 in moderate changes on O₃ concentration within ±2 ppb. The limited changes of
572 climate, BVOCs emissions and foreign anthropogenic emissions will not essentially
573 alter the O₃ formation regime, but may change the O₃ production under the nearly
574 same NO₂ concentration. Changes of individual meteorological factors are expected
575 to easily influence the O₃ and NO₂ concentrations (Pope et al., 2015; Liu and Wang,
576 2020; Dewan and Lakhani, 2022). The modeled little response of NO₂ to
577 meteorological change, except that in the non-warm season for BTH, might be
578 attributed to the compensating effect of different variables. The limited influence of
579 BVOCs on the O₃ formation sensitivity to precursors is consistent with Gao et al.
580 (2022), which reported comparable empirical kinetic modelling approach (EKMA)
581 curves with and without BVOCs emissions. The transboundary O₃ pollution results
582 from the transport of both O₃ and its precursors (mainly associated with PAN), while
583 NO₂ is less influenced by long-range transport due to its shorter lifetime (Ni et al.,
584 2018; Yin et al., 2022).

585 The change in O₃ formation regime might partly explain the finding that the joint
586 effect of multiple factors on restraining O₃ pollution will be larger than the aggregated
587 effects of individual factors. Under a NO_x-limited regime, O₃ is less sensitive to
588 changing VOCs emissions (e.g., BVOCs emissions) than that under a VOC-limited
589 one. Therefore, the enhancement of O₃ due to BVOCs emission growth in the future
590 will be restrained with a much lower NO₂ concentration. This indicates a co-benefit of
591 reducing the anthropogenic emissions to restrain the potential O₃ pollution elevation
592 due to growing BVOCs emissions (as a part of climate penalty) in the future.

593 **3.5 Change of O₃ exceedance events over the east of China**

594 Figure 8 shows the “O₃ exceedance events” over the east of China (mainly
595 including Northern, Eastern, Central and Southern China) in the 2020s and 2060s, and
596 the changes influenced by different factors. The exceedance is defined as number of
597 days with the MDA8 O₃ exceeding the Chinese National Air Quality Standard-Grade
598 II (160 μg m⁻³ or 81.6 ppb). The exceedance events appear mainly in the warm season

599 (Figure S7). Areas with frequent exceedance (over 50 days) in the 2020s were mainly
600 located in Northern China. Much fewer exceedances are found for YRD and PRD
601 (19.3 and 8.2 days in 2020s, respectively). In the 2060s, the O₃ exceedance events
602 will drop significantly. The exceedance days will be fewer than 10 days for most of
603 the country, except for some areas in BTH which will still have more than 20
604 exceedance days over the year.

605 Domestic emission abatement will be the most important factor reducing the O₃
606 exceedance, particularly in Northern China. The exceedance days will be cut by 45.3,
607 19.1 and 8.1 days for BTH, YRD and PRD, respectively, with the maximum reduction
608 reaching 80 days within BTH and YRD. Notably, the spatial pattern of changing O₃
609 exceedance due to emission reduction is different from that of changing MDA8 O₃
610 due to emission reduction as shown in Figure 5a. Even the warm season MDA8 O₃
611 concentration of BTH will decline only 9.7 ppb, the O₃ exceedance events will be
612 greatly reduced, indicating that national emission controls will be especially effective
613 in reducing serious O₃ pollution. Climate change will mainly affect Jiangsu, Anhui,
614 Henan and Hebei provinces, elevating the exceedance by more than 15 days in most
615 of these areas. For YRD and PRD, climate change will elevate the exceedance by 9.5
616 and 3.3 days, respectively. Some areas of BTH will benefit from climate change, with
617 the exceedance declining 0–10 days. The influences of BVOCs and foreign emission
618 change on exceedance days are of limited regional differences, with a growth of 5 to
619 15 days for the former and a decline of –5 to 0 days for the latter. The exceedances
620 elevated by BVOCs emission growth will be 6.6, 6.1 and 2.8 days for BTH, YRD and
621 PRD with the maximum reaching 19, 18 and 12 days within the region, respectively,
622 reflecting an unneglectable role of biogenic source change on future O₃ episodes.

623 **4 Conclusions**

624 We explore the response of China's surface O₃ concentration to the future
625 changes of multiple factors under SSP2-45, based on a series of sensitivity

626 experiments with WRF-MEGAN-CMAQ simulations. From the 2020s to 2060s, the
627 MDA8 O₃ concentration is predicted to decline by 7.7 and 1.1 ppb in the warm and
628 non-warm season, respectively, and the O₃ exceedances of Chinese National Air
629 Quality Standard (Grade II) will be largely eliminated. In the warm season, MDA8 O₃
630 in BTH, YRD and PRD will decline by 9.7, 14.8 and 12.58 ppb, respectively, larger
631 than the national average level. However, MDA8 O₃ will increase in BTH and YRD
632 in the non-warm season attributed to the reduced NO_x emissions and thereby titration
633 effect. The O₃ pollution will expand towards the non-warm season in the future,
634 bringing new challenge for policy makers to optimize the strategy of precursor
635 emission controls based on local conditions.

636 Reduction of local anthropogenic emissions is estimated to dominate the spatial
637 distribution and magnitude of future O₃ change. Meteorological variation will lead to
638 a change of MDA8 O₃ ranging between -1 and 4 ppb for most areas in the warm
639 season. The influences of changing BVOCs and foreign anthropogenic emissions will
640 be within ±3 ppb, with the former elevating O₃ while the latter reducing O₃.
641 Especially in areas with high O₃ pollution and intense NO_x emissions, the growing
642 BVOCs emissions will more enhance the risk of O₃ pollution. The joint effect of
643 multiple factors on restraining O₃ pollution will be larger than the aggregated effects
644 of individual factors, which can be partly explained by the changing O₃ formation
645 regime. Large amount of emission reduction under SSP2-45 will reshape the O₃
646 formation sensitivity to precursors. In BTH and YRD, O₃ formation in the warm
647 season is projected to shift from weak VOC-limited to transitional or NO_x-limited
648 regime, while VOC-limited regime will still dominate in the non-warm season. In the
649 future, O₃ will be less sensitive to BVOCs change in a low NO_x environment along
650 with persistent emission controls, highlighting the benefit of anthropogenic emissions
651 abatement on mitigating the climate penalty and limiting O₃ pollution.

652 Limitations exist in current study. Firstly, the future climate data are taken from
653 one single model CESM, subject to bias in the assessment of meteorological influence

654 on O₃. Secondly, some factors that will influence future O₃ level are not included in
655 our analyses, such as the changing CH₄ concentration, increasing soil NO_x emissions
656 and the stratosphere-troposphere exchange of O₃. For example, the hotspot of soil
657 NO_x emissions in northern China is also the region with high-large reduction of
658 anthropogenic NO_x reductions-emission but relatively small reductionsdecline in O₃
659 concentrations. Under a warmer climate, Thea growing trend of -future
660 increasing-soil NO_x emissions areis expected-to for the future, and may thus present
661 an additional challenge for anthropogenic-NO_xO₃ pollution alleviation.
662 emissions control. -Thirdly, there exist gaps between the downscaled and realistic
663 conditions of meteorology for the 2020s, leading to uncertainty in the O₃ simulation.
664 Finally, the changing O₃ formation regime is presented through the relation between
665 O₃ and NO₂ concentrations, and the mechanism how the climate penalty will
666 influence O₃ formation under substantial reduction of anthropogenic emissions needs
667 to be better analyzed in future studies.

668 **Data availability**

669 All data in this study are available from the authors upon request.

670 **Author contributions**

671 JYang developed the methodology, conducted the work and wrote the draft.
672 YZhao improved the methodology, supervised the work and revised the manuscript.
673 YWang and LZhang contributed to the methodology and provided supports to the
674 scientific interpretation and discussions.

675 **Competing interests**

676 The authors declare that they have no conflict of interest.

677 **Acknowledgments**

678 This work was sponsored by the National Key Research and Development

679 Program of China (2023YFC3709802), National Natural Science Foundation of China
680 (42177080), and the Key Research and Development Programme of Jiangsu Province
681 (BE2022838). We thank Qiang Zhang and Dan Tong from Tsinghua University for
682 the emission data (MEIC and DPEC).

683 **References**

- 684 Akimoto, H. and Tanimoto, H.: Rethinking of the adverse effects of NO_x-control on
685 the reduction of methane and tropospheric ozone – Challenges toward a denitrified
686 society, *Atmos. Environ.*, 277, 119033, 10.1016/j.atmosenv.2022.119033, 2022.
- 687 Andersson, C. and Engardt, M.: European ozone in a future climate: Importance of
688 changes in dry deposition and isoprene emissions, *J. Geophys. Res.-Atmos.*, 115,
689 D02303, 10.1029/2008jd011690, 2010.
- 690 Appel, K. W., Pouliot, G. A., Simon, H., Sarwar, G., Pye, H. O. T., Napelenok, S. L.,
691 Akhtar, F., and Roselle, S. J.: Evaluation of dust and trace metal estimates from the
692 Community Multiscale Air Quality (CMAQ) model version 5.0, *Geosci. Model Dev.*,
693 6, 883–899, 10.5194/gmd-6-883-2013, 2013.
- 694 Avnery, S., Mauzerall, D. L., Liu, J., and Horowitz, L. W.: Global crop yield
695 reductions due to surface ozone exposure: 1. Year 2000 crop production losses and
696 economic damage, *Atmos. Environ.*, 45, 2284–2296, 10.1016/j.atmosenv.2010.11.045,
697 2011.
- 698 Cao, J., Situ, S., Hao, Y., Xie, S., and Li, L.: Enhanced summertime ozone and SOA
699 from biogenic volatile organic compound (BVOC) emissions due to vegetation
700 biomass variability during 1981–2018 in China, *Atmos. Chem. Phys.*, 22, 2351–2364,
701 10.5194/acp-22-2351-2022, 2022.
- 702 Chen, J., Avise, J., Guenther, A., Wiedinmyer, C., Salathe, E., Jackson, R. B., and
703 Lamb, B.: Future land use and land cover influences on regional biogenic emissions
704 and air quality in the United States, *Atmos. Environ.*, 43, 5771–5780,
705 10.1016/j.atmosenv.2009.08.015, 2009.
- 706 Chen, X., Jiang, Z., Shen, Y., Li, R., Fu, Y., Liu, J., Han, H., Liao, H., Cheng, X.,
707 Jones, D. B. A., Worden, H., and Abad, G. G.: Chinese Regulations Are
708 Working—Why Is Surface Ozone Over Industrialized Areas Still High? Applying

709 Lessons From Northeast US Air Quality Evolution, *Geophys. Res. Lett.*, 48,
710 e2021GL092816, 10.1029/2021gl092816, 2021.

711 [Chen, X., Wang, M., He, T. L., Jiang, Z., Zhang, Y., Zhou, L., Liu, J., Liao, H.,](#)
712 [Worden, H., Jones, D., Chen, D., Tan, Q., and Shen, Y.: Data- and Model-Based](#)
713 [Urban O3 Responses to NOx Changes in China and the United States, *J. Geophys.*](#)
714 [Res.-Atmos.](#), 128, e2022JD038228, 10.1029/2022jd038228, 2023.

715 Cheng, J., Tong, D., Liu, Y., Yu, S., Yan, L., Zheng, B., Geng, G., He, K., and Zhang,
716 Q.: Comparison of Current and Future PM_{2.5} Air Quality in China Under CMIP6 and
717 DPEC Emission Scenarios, *Geophys. Res. Lett.*, 48, e2021GL093197,
718 10.1029/2021gl093197, 2021a.

719 Cheng, J., Tong, D., Zhang, Q., Liu, Y., Lei, Y., Yan, G., Yan, L., Yu, S., Cui, R. Y.,
720 Clarke, L., Geng, G., Zheng, B., Zhang, X., Davis, S. J., and He, K.: Pathways of
721 China's PM_{2.5} air quality 2015–2060 in the context of carbon neutrality, *Natl. Sci.*
722 *Rev.*, 8, nwab078, 10.1093/nsr/nwab078, 2021b.

723 [Coumou, D., Di Capua, G., Vavrus, S., Wang, L., and Wang, S.: The influence of](#)
724 [Arctic amplification on mid-latitude summer circulation, *Nat. Commun.*, 9,](#)
725 [10.1038/s41467-018-05256-8, 2018.](#)

726 [Deng, H., Hua, W., and Fan, G.: Evaluation and Projection of Near-Surface Wind](#)
727 [Speed over China Based on CMIP6 Models, *Atmosphere*, 12,](#)
728 [10.3390/atmos12081062, 2021.](#)

729 Dewan, S. and Lakhani, A.: Tropospheric ozone and its natural precursors impacted
730 by climatic changes in emission and dynamics, *Front. Environ. Sci.*, 10, 1007942,
731 10.3389/fenvs.2022.1007942, 2022.

732 Feng, Y., Ning, M., Xue, W., Cheng, M., and Lei, Y.: Developing China's roadmap
733 for air quality improvement: A review on technology development and future
734 prospects, *J. Environ. Sci.*, 123, 510–521, 10.1016/j.jes.2022.10.028, 2023.

735 Feng, Z. Z., Xu, Y. S., Kobayashi, K., Dai, L. L., Zhang, T. Y., Agathokleous, E.,
736 Calatayud, V., Paoletti, E., Mukherjee, A., Agrawal, M., Park, R. J., Oak, Y. J., and
737 Yue, X.: Ozone pollution threatens the production of major staple crops in East Asia,
738 *Nat. Food*, 3, 47–56, [10.1038/s43016-021-00422-6](https://doi.org/10.1038/s43016-021-00422-6), 2022.

739 FinlaysonPitts, B. J. and Pitts, J. N.: Tropospheric air pollution: Ozone, airborne
740 toxics, polycyclic aromatic hydrocarbons, and particles, *Science*, 276, 1045–1052,
741 [10.1126/science.276.5315.1045](https://doi.org/10.1126/science.276.5315.1045), 1997.

742 Fischer, E. V., Jacob, D. J., Yantosca, R. M., Sulprizio, M. P., Millet, D. B., Mao, J.,
743 Paulot, F., Singh, H. B., Roiger, A., Ries, L., Talbot, R. W., Dzepina, K., and Pandey
744 Deolal, S.: Atmospheric peroxyacetyl nitrate (PAN): a global budget and source
745 attribution, *Atmos. Chem. Phys.*, 14, 2679–2698, [10.5194/acp-14-2679-2014](https://doi.org/10.5194/acp-14-2679-2014), 2014.

746 Gao, M., Gao, J., Zhu, B., Kumar, R., Lu, X., Song, S., Zhang, Y., Jia, B., Wang, P.,
747 Beig, G., Hu, J., Ying, Q., Zhang, H., Sherman, P., and McElroy, M. B.: Ozone
748 pollution over China and India: seasonality and sources, *Atmos. Chem. Phys.*, 20,
749 4399–4414, [10.5194/acp-20-4399-2020](https://doi.org/10.5194/acp-20-4399-2020), 2020.

750 Gao, M., Wang, F., Ding, Y., Wu, Z., Xu, Y., Lu, X., Wang, Z., Carmichael, G. R.,
751 and McElroy, M. B.: Large-scale climate patterns offer preseasonal hints on the
752 co-occurrence of heat wave and O₃ pollution in China, *Proc. Natl. Acad. Sci. U.S.A.*,
753 120, e2218274120, [10.1073/pnas.2218274120](https://doi.org/10.1073/pnas.2218274120), 2023.

754 Gao, Y., Fu, J. S., Drake, J. B., Lamarque, J. F., and Liu, Y.: The impact of emission
755 and climate change on ozone in the United States under representative concentration
756 pathways (RCPs), *Atmos. Chem. Phys.*, 13, 9607–9621, [10.5194/acp-13-9607-2013](https://doi.org/10.5194/acp-13-9607-2013),
757 2013.

758 Gao, Y., Yan, F., Ma, M., Ding, A., Liao, H., Wang, S., Wang, X., Zhao, B., Cai, W.,
759 Su, H., Yao, X., and Gao, H.: Unveiling the dipole synergic effect of biogenic and
760 anthropogenic emissions on ozone concentrations, *Sci. Total. Env.*, 818, 151722,

761 10.1016/j.scitotenv.2021.151722, 2022.

762 Gidden, M. J., Riahi, K., Smith, S. J., Fujimori, S., Luderer, G., Kriegler, E., van
763 Vuuren, D. P., van den Berg, M., Feng, L., Klein, D., Calvin, K., Doelman, J. C.,
764 Frank, S., Fricko, O., Harmsen, M., Hasegawa, T., Havlik, P., Hilaire, J., Hoesly, R.,
765 Horing, J., Popp, A., Stehfest, E., and Takahashi, K.: Global emissions pathways
766 under different socioeconomic scenarios for use in CMIP6: a dataset of harmonized
767 emissions trajectories through the end of the century, *Geosci. Model Dev.*, 12, 1443–
768 1475, 10.5194/gmd-12-1443-2019, 2019.

769 Gong, C. and Liao, H.: A typical weather pattern for ozone pollution events in North
770 China, *Atmos. Chem. Phys.*, 19, 13725–13740, 10.5194/acp-19-13725-2019, 2019.

771 Gonzalez-Abraham, R., Chung, S. H., Avise, J., Lamb, B., Salathe, E. P., Jr., Nolte, C.
772 G., Loughlin, D., Guenther, A., Wiedinmyer, C., Duhl, T., Zhang, Y., and Streets, D.
773 G.: The effects of global change upon United States air quality, *Atmos. Chem. Phys.*,
774 15, 12645–12665, 10.5194/acp-15-12645-2015, 2015.

775 Guenther, A. B., Jiang, X., Heald, C. L., Sakulyanontvittaya, T., Duhl, T., Emmons, L.
776 K., and Wang, X.: The Model of Emissions of Gases and Aerosols from Nature
777 version 2.1 (MEGAN2.1): an extended and updated framework for modeling biogenic
778 emissions, *Geosci. Model Dev.*, 5, 1471–1492, 10.5194/gmd-5-1471-2012, 2012.

779 Han, H., Liu, J., Yuan, H., Wang, T., Zhuang, B., and Zhang, X.: Foreign influences
780 on tropospheric ozone over East Asia through global atmospheric transport, *Atmos.*
781 *Chem. Phys.*, 19, 12495–12514, 10.5194/acp-19-12495-2019, 2019.

782 Han, H., Liu, J., Shu, L., Wang, T., and Yuan, H.: Local and synoptic meteorological
783 influences on daily variability in summertime surface ozone in eastern China, *Atmos.*
784 *Chem. Phys.*, 20, 203–222, 10.5194/acp-20-203-2020, 2020.

785 Harper, K. L. and Unger, N.: Global climate forcing driven by altered BVOC fluxes
786 from 1990 to 2010 land cover change in maritime Southeast Asia, *Atmos. Chem.*

787 Phys., 18, 16931–16952, 10.5194/acp-18-16931-2018, 2018.

788 Hollaway, M. J., Arnold, S. R., Collins, W. J., Folberth, G., and Rap, A.: Sensitivity
789 of midnineteenth century tropospheric ozone to atmospheric chemistry - vegetation
790 interactions, *J. Geophys. Res.-Atmos.*, 122, 2452–2473, 10.1002/2016jd025462,
791 2017.

792 Hong, C., Zhang, Q., Zhang, Y., Davis, S. J., Tong, D., Zheng, Y., Liu, Z., Guan, D.,
793 He, K., and Schellnhuber, H. J.: Impacts of climate change on future air quality and
794 human health in China, *Proc. Natl. Acad. Sci. U.S.A.*, 116, 17193–17200,
795 10.1073/pnas.1812881116, 2019.

796 [Hou, X., Wild, O., Zhu, B., and Lee, J.: Future tropospheric ozone budget and](#)
797 [distribution over east Asia under a net-zero scenario, *Atmos. Chem. Phys.*, 23, 15395–](#)
798 [15411, 10.5194/acp-23-15395-2023, 2023.](#)

799 Hu, A., Xie, X., Gong, K., Hou, Y., Zhao, Z., and Hu, J.: Assessing the Impacts of
800 Climate Change on Meteorology and Air Stagnation in China Using a Dynamical
801 Downscaling Method, *Front. Environ. Sci.*, 10, 894887, 10.3389/fenvs.2022.894887,
802 2022.

803 Hu, J., Chen, J., Ying, Q., and Zhang, H.: One-year simulation of ozone and
804 particulate matter in China using WRF/CMAQ modeling system, *Atmos. Chem.*
805 *Phys.*, 16, 10333–10350, 10.5194/acp-16-10333-2016, 2016.

806 Hurtt, G. C., Chini, L., Sahajpal, R., Frohking, S., Boudris, B. L., Calvin, K.,
807 Doelman, J. C., Fisk, J., Fujimori, S., Klein Goldewijk, K., Hasegawa, T., Havlik, P.,
808 Heinemann, A., Humpenöder, F., Jungclaus, J., Kaplan, J. O., Kennedy, J., Krisztin, T.,
809 Lawrence, D., Lawrence, P., Ma, L., Mertz, O., Pongratz, J., Popp, A., Poulter, B.,
810 Riahi, K., Shevliakova, E., Stehfest, E., Thornton, P., Tubiello, F. N., van Vuuren, D.
811 P., and Zhang, X.: Harmonization of global land use change and management for the
812 period 850–2100 (LUH2) for CMIP6, *Geosci. Model Dev.*, 13, 5425–5464,

813 10.5194/gmd-13-5425-2020, 2020.

814 IPCC: Climate Change 2021 – The Physical Science Basis: Working Group I
815 Contribution to the Sixth Assessment Report of the Intergovernmental Panel on
816 Climate Change, Cambridge University Press, Cambridge, 10.1017/9781009157896,
817 2021.

818 IPCC: Climate Change 2022: Mitigation of Climate Change: Working Group III
819 Contribution to the Sixth Assessment Report of the Intergovernmental Panel on
820 Climate Change, Cambridge University Press, Cambridge, 10.1017/9781009157926,
821 2022.

822 Jerrett, M., Burnett, R. T., Pope, C. A., 3rd, Ito, K., Thurston, G., Krewski, D., Shi, Y.,
823 Calle, E., and Thun, M.: Long-term ozone exposure and mortality, *N. Engl. J .Med.*,
824 360, 1085–1095, 10.1056/NEJMoa0803894, 2009.

825 Jiang, Y., Ding, D., Dong, Z., Liu, S., Chang, X., Zheng, H., Xing, J., and Wang, S.:
826 Extreme Emission Reduction Requirements for China to Achieve World Health
827 Organization Global Air Quality Guidelines, *Environ. Sci. Technol.*, 57, 4424–4433,
828 10.1021/acs.est.2c09164, 2023.

829 Jin, X. and Holloway, T.: Spatial and temporal variability of ozone sensitivity over
830 China observed from the Ozone Monitoring Instrument, *J. Geophys. Res.-Atmos.*, 120,
831 7229–7246, 10.1002/2015jd023250, 2015.

832 [Kong, L., Song, M., Li, X., Liu, Y., Lu, S., Zeng, L., and Zhang, Y.: Analysis of](#)
833 [China's PM\(2.5\) and ozone coordinated control strategy based on the observation data](#)
834 [from 2015 to 2020, *J. Environ. Sci. \(China\)*, 138, 385–394, 10.1016/j.jes.2023.03.030,](#)
835 [2024.](#)

836 [Lelieveld, J., Evans, J. S., Fnais, M., Giannadaki, D., and Pozzer, A.: The contribution](#)
837 [of outdoor air pollution sources to premature mortality on a global scale, *Nature*, 525,](#)
838 [367–371, 10.1038/nature15371, 2015.](#)

839 Li, H., Yang, Y., Jin, J., Wang, H., Li, K., Wang, P., and Liao, H.: Climate-driven
840 deterioration of future ozone pollution in Asia predicted by machine learning with
841 multi-source data, *Atmos. Chem. Phys.*, 23, 1131–1145, 10.5194/acp-23-1131-2023,
842 2023.

843 Li, K., Jacob, D. J., Shen, L., Lu, X., De Smedt, I., and Liao, H.: Increases in surface
844 ozone pollution in China from 2013 to 2019: anthropogenic and meteorological
845 influences, *Atmos. Chem. Phys.*, 20, 11423–11433, 10.5194/acp-20-11423-2020,
846 2020a.

847 Li, K., Jacob, D. J., Liao, H., Qiu, Y., Shen, L., Zhai, S., Bates, K. H., Sulprizio, M. P.,
848 Song, S., Lu, X., Zhang, Q., Zheng, B., Zhang, Y., Zhang, J., Lee, H. C., and Kuk, S.
849 K.: Ozone pollution in the North China Plain spreading into the late-winter haze
850 season, *Proc. Natl. Acad. Sci. U.S.A.*, 118, e2015797118, 10.1073/pnas.2015797118,
851 2021.

852 Li, L., Yang, W., Xie, S., and Wu, Y.: Estimations and uncertainty of biogenic
853 volatile organic compound emission inventory in China for 2008-2018, *Sci. Total.*
854 *Env.*, 733, 139301, 10.1016/j.scitotenv.2020.139301, 2020b.

855 Li, M., Zhang, Q., Kurokawa, J.-i., Woo, J.-H., He, K., Lu, Z., Ohara, T., Song, Y.,
856 Streets, D. G., Carmichael, G. R., Cheng, Y., Hong, C., Huo, H., Jiang, X., Kang, S.,
857 Liu, F., Su, H., and Zheng, B.: MIX: a mosaic Asian anthropogenic emission
858 inventory under the international collaboration framework of the MICS-Asia and
859 HTAP, *Atmos. Chem. Phys.*, 17, 935–963, 10.5194/acp-17-935-2017, 2017.

860 Liang, S., Cheng, J., Jia, K., Jiang, B., Liu, Q., Xiao, Z., Yao, Y., Yuan, W., Zhang,
861 X., Zhao, X., and Zhou, J.: The Global Land Surface Satellite (GLASS) Product Suite,
862 *Bull. Am. Meteorol. Soc.*, 102, E323–E337, 10.1175/bams-d-18-0341.1, 2021.

863 Liao, W., Liu, X., Xu, X., Chen, G., Liang, X., Zhang, H., and Li, X.: Projections of
864 land use changes under the plant functional type classification in different SSP-RCP

865 scenarios in China, *Sci. Bull.*, 65, 1935–1947, 10.1016/j.scib.2020.07.014, 2020.

866 Liu, Q., Lam, K. S., Jiang, F., Wang, T. J., Xie, M., Zhuang, B. L., and Jiang, X. Y.:
867 A numerical study of the impact of climate and emission changes on surface ozone
868 over South China in autumn time in 2000–2050, *Atmos. Environ.*, 76, 227–237,
869 10.1016/j.atmosenv.2013.01.030, 2013.

870 Liu, S., Xing, J., Zhang, H., Ding, D., Zhang, F., Zhao, B., Sahu, S. K., and Wang, S.:
871 Climate-driven trends of biogenic volatile organic compound emissions and their
872 impacts on summertime ozone and secondary organic aerosol in China in the 2050s,
873 *Atmos. Environ.*, 218, 117020, 10.1016/j.atmosenv.2019.117020, 2019.

874 Liu, S., Sahu, S. K., Zhang, S., Liu, S., Sun, Y., Liu, X., Xing, J., Zhao, B., Zhang, H.,
875 and Wang, S.: Impact of Climate-Driven Land-Use Change on O₃ and PM Pollution
876 by Driving BVOC Emissions in China in 2050, *Atmosphere*, 13, 1086,
877 10.3390/atmos13071086, 2022.

878 Liu, Y. and Wang, T.: Worsening urban ozone pollution in China from 2013 to
879 2017-Part 1: The complex and varying roles of meteorology, *Atmos. Chem. Phys.*, 20,
880 6305–6321, 10.5194/acp-20-6305-2020, 2020.

881 Liu, Y., Geng, G., Cheng, J., Liu, Y., Xiao, Q., Liu, L., Shi, Q., Tong, D., He, K., and
882 Zhang, Q.: Drivers of Increasing Ozone during the Two Phases of Clean Air Actions
883 in China 2013–2020, *Environ. Sci. Technol.*, 57, 8954–8964, 10.1021/acs.est.3c00054,
884 2023a.

885 [Liu, Z., Wild, O., Doherty, R. M., O'Connor, F. M., and Turnock, S. T.: Benefits of](#)
886 [net-zero policies for future ozone pollution in China, *Atmos. Chem. Phys.*, 23, 13755–](#)
887 [13768, 10.5194/acp-23-13755-2023, 2023b.](#)

888 Lu, X., Zhang, L., and Shen, L.: Meteorology and Climate Influences on Tropospheric
889 Ozone: a Review of Natural Sources, Chemistry, and Transport Patterns, *Curr. Pollut.*
890 *Rep.*, 5, 238–260, 10.1007/s40726-019-00118-3, 2019.

891 Meinshausen, M., Nicholls, Z. R. J., Lewis, J., Gidden, M. J., Vogel, E., Freund, M.,
892 Beyerle, U., Gessner, C., Nauels, A., Bauer, N., Canadell, J. G., Daniel, J. S., John, A.,
893 Krummel, P. B., Luderer, G., Meinshausen, N., Montzka, S. A., Rayner, P. J.,
894 Reimann, S., Smith, S. J., van den Berg, M., Velders, G. J. M., Vollmer, M. K., and
895 Wang, R. H. J.: The shared socio-economic pathway (SSP) greenhouse gas
896 concentrations and their extensions to 2500, *Geosci. Model Dev.*, 13, 3571–3605,
897 [10.5194/gmd-13-3571-2020](https://doi.org/10.5194/gmd-13-3571-2020), 2020.

898 Monaghan, A. J., Steinhoff, D. F., Bruyere, C. L., and Yates, D.: NCAR CESM
899 Global Bias-Corrected CMIP5 Output to Support WRF/MPAS Research, Research
900 Data Archive at the National Center for Atmospheric Research, Computational and
901 Information Systems Laboratory [dataset], [10.5065/D6DJ5CN4](https://doi.org/10.5065/D6DJ5CN4), 2014.

902 Monks, P. S., Archibald, A. T., Colette, A., Cooper, O., Coyle, M., Derwent, R.,
903 Fowler, D., Granier, C., Law, K. S., Mills, G. E., Stevenson, D. S., Tarasova, O.,
904 Thouret, V., von Schneidmesser, E., Sommariva, R., Wild, O., and Williams, M. L.:
905 Tropospheric ozone and its precursors from the urban to the global scale from air
906 quality to short-lived climate forcer, *Atmos. Chem. Phys.*, 15, 8889–8973,
907 [10.5194/acp-15-8889-2015](https://doi.org/10.5194/acp-15-8889-2015), 2015.

908 Ni, R., Lin, J., Yan, Y., and Lin, W.: Foreign and domestic contributions to
909 springtime ozone over China, *Atmos. Chem. Phys.*, 18, 11447–11469,
910 [10.5194/acp-18-11447-2018](https://doi.org/10.5194/acp-18-11447-2018), 2018.

911 [Niu, Y., Zhou, Y., Chen, R., Yin, P., Meng, X., Wang, W., Liu, C., Ji, J. S., Qiu, Y.,](#)
912 [Kan, H., and Zhou, M.: Long-term exposure to ozone and cardiovascular mortality in](#)
913 [China: a nationwide cohort study, *Lancet Planet. Health*, 6, e496–e503,](#)
914 [\[10.1016/s2542-5196\\(22\\)00093-6\]\(https://doi.org/10.1016/s2542-5196\(22\)00093-6\), 2022.](#)

915 O'Neill, B. C., Tebaldi, C., van Vuuren, D. P., Eyring, V., Friedlingstein, P., Hurtt, G.,
916 Knutti, R., Kriegler, E., Lamarque, J.-F., Lowe, J., Meehl, G. A., Moss, R., Riahi, K.,
917 and Sanderson, B. M.: The Scenario Model Intercomparison Project (ScenarioMIP)

918 for CMIP6, *Geosci. Model Dev.*, 9, 3461–3482, 10.5194/gmd-9-3461-2016, 2016.

919 Penuelas, J. and Llusia, J.: BVOCs: plant defense against climate warming?, *Trends*
920 *Plant Sci.*, 8, 105–109, 10.1016/s1360-1385(03)00008-6, 2003.

921 Penuelas, J. and Staudt, M.: BVOCs and global change, *Trends Plant Sci.*, 15, 133–
922 144, 10.1016/j.tplants.2009.12.005, 2010.

923 Pope, R. J., Savage, N. H., Chipperfield, M. P., Ordóñez, C., and Neal, L. S.: The
924 influence of synoptic weather regimes on UK air quality: regional model studies of
925 tropospheric column NO₂, *Atmos. Chem. Phys.*, 15, 11201–11215,
926 10.5194/acp-15-11201-2015, 2015.

927 Porter, W. C. and Heald, C. L.: The mechanisms and meteorological drivers of the
928 summertime ozone–temperature relationship, *Atmos. Chem. Phys.*, 19, 13367–13381,
929 10.5194/acp-19-13367-2019, 2019.

930 Riahi, K., van Vuuren, D. P., Kriegler, E., Edmonds, J., O'Neill, B. C., Fujimori, S.,
931 Bauer, N., Calvin, K., Dellink, R., Fricko, O., Lutz, W., Popp, A., Cuaresma, J. C., Kc,
932 S., Leimbach, M., Jiang, L., Kram, T., Rao, S., Emmerling, J., Ebi, K., Hasegawa, T.,
933 Havlik, P., Humpenöder, F., Da Silva, L. A., Smith, S., Stehfest, E., Bosetti, V., Eom,
934 J., Gernaat, D., Masui, T., Rogelj, J., Strefler, J., Drouet, L., Krey, V., Luderer, G.,
935 Harmsen, M., Takahashi, K., Baumstark, L., Doelman, J. C., Kainuma, M., Klimont,
936 Z., Marangoni, G., Lotze-Campen, H., Obersteiner, M., Tabeau, A., and Tavoni, M.:
937 The Shared Socioeconomic Pathways and their energy, land use, and greenhouse gas
938 emissions implications: An overview, *Glob. Environ. Change*, 42, 153–168,
939 10.1016/j.gloenvcha.2016.05.009, 2017.

940 Schroeder, J. R., Crawford, J. H., Fried, A., Walega, J., Weinheimer, A., Wisthaler, A.,
941 Müller, M., Mikoviny, T., Chen, G., Shook, M., Blake, D. R., and Tonnesen, G. S.:
942 New insights into the column CH₂O/NO₂ ratio as an indicator of near-surface ozone
943 sensitivity, *J. Geophys. Res.-Atmos.*, 122, 8885–8907, 10.1002/2017jd026781, 2017.

944 Shi, X., Zheng, Y., Lei, Y., Xue, W., Yan, G., Liu, X., Cai, B., Tong, D., and Wang, J.:
945 Air quality benefits of achieving carbon neutrality in China, *Sci. Total. Env.*, 795,
946 148784, 10.1016/j.scitotenv.2021.148784, 2021.

947 Sillman, S. and He, D.: Some theoretical results concerning O₃ - NO_x-VOC chemistry
948 and NO_x-VOC indicators, *J. Geophys. Res.-Atmos.*, 107, 4659,
949 10.1029/2001jd001123, 2002.

950 Sheffield, J. and Wood, E. F.: Projected changes in drought occurrence under future
951 global warming from multi-model, multi-scenario, IPCC AR4 simulations, *Clim.*
952 *Dyn.*, 31, 79–105, 10.1007/s00382-007-0340-z, 2008.

953 Szogs, S., Arneth, A., Anthoni, P., Doelman, J. C., Humpenöder, F., Popp, A., Pugh,
954 T. A. M., and Stehfest, E.: Impact of LULCC on the emission of BVOCs during the
955 21st century, *Atmos. Environ.*, 165, 73–87, 10.1016/j.atmosenv.2017.06.025, 2017.

956 Tai, A. P. K. and Val Martin, M.: Impacts of ozone air pollution and temperature
957 extremes on crop yields: Spatial variability, adaptation and implications for future
958 food security, *Atmos. Environ.*, 169, 11–21, 10.1016/j.atmosenv.2017.09.002, 2017.

959 Tong, D., Cheng, J., Liu, Y., Yu, S., Yan, L., Hong, C. P., Qin, Y., Zhao, H. Y.,
960 Zheng, Y. X., Geng, G. N., Li, M., Liu, F., Zhang, Y. X., Zheng, B., Clarke, L., and
961 Zhang, Q.: Dynamic projection of anthropogenic emissions in China: methodology
962 and 2015-2050 emission pathways under a range of socio-economic, climate policy,
963 and pollution control scenarios, *Atmos. Chem. Phys.*, 20, 5729–5757,
964 10.5194/acp-20-5729-2020, 2020.

965 van Vuuren, D. P., Edmonds, J., Kainuma, M., Riahi, K., Thomson, A., Hibbard, K.,
966 Hurtt, G. C., Kram, T., Krey, V., Lamarque, J. F., Masui, T., Meinshausen, M.,
967 Nakicenovic, N., Smith, S. J., and Rose, S. K.: The representative concentration
968 pathways: an overview, *Clim. Change*, 109, 5–31, 10.1007/s10584-011-0148-z, 2011.

969 von Schneidmesser, E., Monks, P. S., Allan, J. D., Bruhwiler, L., Forster, P., Fowler,

970 D., Lauer, A., Morgan, W. T., Paasonen, P., Righi, M., Sindelarova, K., and Sutton,
971 M. A.: Chemistry and the Linkages between Air Quality and Climate Change, *Chem.*
972 *Rev.*, 115, 3856–3897, 10.1021/acs.chemrev.5b00089, 2015.

973 Wang, H., Wu, Q., Guenther, A. B., Yang, X., Wang, L., Xiao, T., Li, J., Feng, J., Xu,
974 Q., and Cheng, H.: A long-term estimation of biogenic volatile organic compound
975 (BVOC) emission in China from 2001–2016: the roles of land cover change and
976 climate variability, *Atmos. Chem. Phys.*, 21, 4825–4848, 10.5194/acp-21-4825-2021,
977 2021a.

978 Wang, L., Tai, A. P. K., Tam, C.-Y., Sadiq, M., Wang, P., and Cheung, K. K. W.:
979 Impacts of future land use and land cover change on mid-21st-century surface ozone
980 air quality: distinguishing between the biogeophysical and biogeochemical effects,
981 *Atmos. Chem. Phys.*, 20, 11349–11369, 10.5194/acp-20-11349-2020, 2020.

982 Wang, N., Xu, J., Pei, C., Tang, R., Zhou, D., Chen, Y., Li, M., Deng, X., Deng, T.,
983 Huang, X., and Ding, A.: Air Quality During COVID-19 Lockdown in the Yangtze
984 River Delta and the Pearl River Delta: Two Different Responsive Mechanisms to
985 Emission Reductions in China, *Environ. Sci. Technol.*, 55, 5721–5730,
986 10.1021/acs.est.0c08383, 2021b.

987 Wang, P., Yang, Y., Li, H., Chen, L., Dang, R., Xue, D., Li, B., Tang, J., Leung, L. R.,
988 and Liao, H.: North China Plain as a hot spot of ozone pollution exacerbated by
989 extreme high temperatures, *Atmos. Chem. Phys.*, 22, 4705–4719,
990 10.5194/acp-22-4705-2022, 2022.

991 Wang, Y., Zhao, Y., Liu, Y., Jiang, Y., Zheng, B., Xing, J., Liu, Y., Wang, S., and
992 Nielsen, C. P.: Sustained emission reductions have restrained the ozone pollution over
993 China, *Nat. Geosci.*, 10.1038/s41561-023-01284-2, 2023.

994 Weng, X., Forster, G. L., and Nowack, P.: A machine learning approach to quantify
995 meteorological drivers of ozone pollution in China from 2015 to 2019, *Atmos. Chem.*

996 Phys., 22, 8385–8402, 10.5194/acp-22-8385-2022, 2022.

997 Wu, K., Yang, X., Chen, D., Gu, S., Lu, Y., Jiang, Q., Wang, K., Ou, Y., Qian, Y.,
998 Shao, P., and Lu, S.: Estimation of biogenic VOC emissions and their corresponding
999 impact on ozone and secondary organic aerosol formation in China, Atmos. Res., 231,
1000 104656, 10.1016/j.atmosres.2019.104656, 2020a.

1001 Wu, J., Shi, Y., and Xu, Y.: Evaluation and Projection of Surface Wind Speed Over
1002 China Based on CMIP6 GCMs, J. Geophys. Res.-Atmos., 125,
1003 10.1029/2020jd033611, 2020b.

1004 Xiao, Q., Geng, G., Xue, T., Liu, S., Cai, C., He, K., and Zhang, Q.: Tracking PM_{2.5}
1005 and O₃ Pollution and the Related Health Burden in China 2013–2020, Environ. Sci.
1006 Technol., 56, 6922–6932, 10.1021/acs.est.1c04548, 2022.

1007 Xu, B., Wang, T., Ma, D., Song, R., Zhang, M., Gao, L., Li, S., Zhuang, B., Li, M.,
1008 and Xie, M.: Impacts of regional emission reduction and global climate change on air
1009 quality and temperature to attain carbon neutrality in China, Atmos. Res., 279,
1010 106384, 10.1016/j.atmosres.2022.106384, 2022.

1011 Yang, J. and Zhao, Y.: Performance and application of air quality models on ozone
1012 simulation in China – A review, Atmos. Environ., 293, 119446,
1013 10.1016/j.atmosenv.2022.119446, 2023.

1014 Yao, Y., Zou, X., Zhao, Y., and Wang, T.: Rapid Changes in Land-Sea Thermal
1015 Contrast Across China's Coastal Zone in a Warming Climate, J. Geophys.
1016 Res.-Atmos., 124, 2049-2067, 10.1029/2018jd029347, 2019.

1017 Yarwood, G., Rao, S., Yocke, M., and Whitten, G.: Updates to the Carbon Bond
1018 Mechanism: CB05, Yocke and Company Final Rep. to the U.S, 2005.

1019 Yin, H., Sun, Y., Notholt, J., Palm, M., and Liu, C.: Spaceborne tropospheric nitrogen
1020 dioxide (NO₂) observations from 2005–2020 over the Yangtze River Delta (YRD),
1021 China: variabilities, implications, and drivers, Atmos. Chem. Phys., 22, 4167–4185,

1022 10.5194/acp-22-4167-2022, 2022.

1023 [Yin, P., Brauer, M., Cohen, A. J., Wang, H., Li, J., Burnett, R. T., Stanaway, J. D.,](#)
1024 [Causey, K., Larson, S., Godwin, W., Frostad, J., Marks, A., Wang, L., Zhou, M., and](#)
1025 [Murray, C. J. L.: The effect of air pollution on deaths, disease burden, and life](#)
1026 [expectancy across China and its provinces, 1990–2017: an analysis for the Global](#)
1027 [Burden of Disease Study 2017, Lancet Planet. Health, 4, e386–e398,](#)
1028 [10.1016/s2542-5196\(20\)30161-3, 2020.](#)

1029 Zheng, B., Tong, D., Li, M., Liu, F., Hong, C. P., Geng, G. N., Li, H. Y., Li, X., Peng,
1030 L. Q., Qi, J., Yan, L., Zhang, Y. X., Zhao, H. Y., Zheng, Y. X., He, K. B., and Zhang,
1031 Q.: Trends in China's anthropogenic emissions since 2010 as the consequence of clean
1032 air actions, Atmos. Chem. Phys., 18, 14095–14111, 10.5194/acp-18-14095-2018,
1033 2018.

1034 Zhu, J. and Liao, H.: Future ozone air quality and radiative forcing over China owing
1035 to future changes in emissions under the Representative Concentration Pathways
1036 (RCPs), J. Geophys. Res.-Atmos., 121, 1978–2001, 10.1002/2015jd023926, 2016.

1037 Zhu, J., Tai, A. P. K., and Hung Lam Yim, S.: Effects of ozone–vegetation
1038 interactions on meteorology and air quality in China using a two-way coupled land–
1039 atmosphere model, Atmos. Chem. Phys., 22, 765–782, 10.5194/acp-22-765-2022,
1040 2022.

1041

1042 **FIGURE CAPTIONS**

1043 Figure 1 The modelling domain and geographical definitions (denoted by colors) of
1044 this study. Boundaries of the three regions, including BTH (Beijing-Tianjin-Hebei),
1045 YRD (Yangtze River Delta) and PRD (Pearl River Delta), are marked by dark grey
1046 lines.

1047 Figure 2 Projected changes of the ~~strongly~~ ozone-related meteorological
1048 ~~elements~~factors, including daily maximum temperature at 2 m (T-max, a and d),
1049 relative humidity (RH, b and e) and wind speed (WS, c and f), from the 2020s to
1050 2060s. Panels (a-c) represent those of the warm season, and panels (d-f) represent
1051 those of non-warm season.

1052 Figure 3 Simulation and projection of seasonal average MDA8 O₃ in the 2020s
1053 (Case1, a and b) and 2060s (Case2, d and e), and the changes over this period
1054 (Case2–Case1, c and f). Panels (a-c) represent those of the warm season, and panels
1055 (d-f) represent those of non-warm season. Regional mean concentrations across China
1056 (CHN), BTH, YRD and PRD are inset.

1057 Figure 4 Simulation and projection of monthly average MDA8 O₃ in the 2020s and
1058 2060s across CHN (a), BTH (b), YRD (c) and PRD (d).

1059 Figure 5 Projected changes of MDA8 O₃ from the 2020s to 2060s attributed to
1060 anthropogenic emissions from local sources (Case3–Case1, a and e), meteorological
1061 conditions (Case4–Case1, b and f), BVOCs emissions (Case5–Case1, c and g) and
1062 anthropogenic emissions from surrounding countries (Case6–Case1, d and h). Panels
1063 (a-d) represent those of the warm season, and panels (e-h) represent those of
1064 non-warm season. Regional mean changes across CHN, BTH, YRD and PRD are
1065 inset.

1066 Figure 6 The relationships between the separate MDA8 O₃ changes attributed to the

1067 four factors (denoted by the name of Case3–6) and the total changes from the 2020s
1068 to 2060s over China and the three regions. Panels (a-d) represent those of the warm
1069 season, and panels (e-h) represent those of non-warm season. The relative
1070 contributions of the four factors to the total influence of future change are shown in
1071 the light grey box.

1072 Figure 7 The relationships between simulated hourly NO₂ and O₃ concentrations with
1073 the lognormal fits for different regions and seasons. The colored circles, representing
1074 different cases, come from the seasonal average concentrations for each grid in the
1075 target region. The specific circles with black border represent the regional average
1076 situation, and the turning points of every fitted curve are marked by the “+” sign. The
1077 density plots of the 2020s and 2060s are inset.

1078 Figure 8 Projected annual O₃ exceedance over the east of China in the 2020s and
1079 2060s, and the exceedance changes when the four factors at 2060s level. Regional
1080 mean changes across CHN, BTH, YRD and PRD are inset.

1081

1082 **TABLES**

1083 **Table 1-** List of simulation cases to investigate the impact of future change upon
 1084 surface O₃ in China, with sensitivity experiments from the perspectives of four
 1085 main influencing factors.

Case number	Case name	China's local emissions	Meteorological conditions	BVOCs emissions	Surrounding emissions
Case1	2020s	2020	2018-2022	2018-2022	2020
Case2	2060s	2060	2058-2062	2058-2062	2060
Case3	EMIS	2060	2018-2022	2018-2022	2020
Case4	CLIM	2020	2058-2062	2018-2022	2020
Case5	BVOC	2020	2018-2022	2058-2062	2020
Case6	SURR	2020	2018-2022	2018-2022	2060

1086

1087

1088 **Table 2-** The BVOCs estimation over China and emission intensity in BTH, YRD
 1089 and PRD of the 2020s and 2060s, as well as the corresponding growth rates over
 1090 this period.

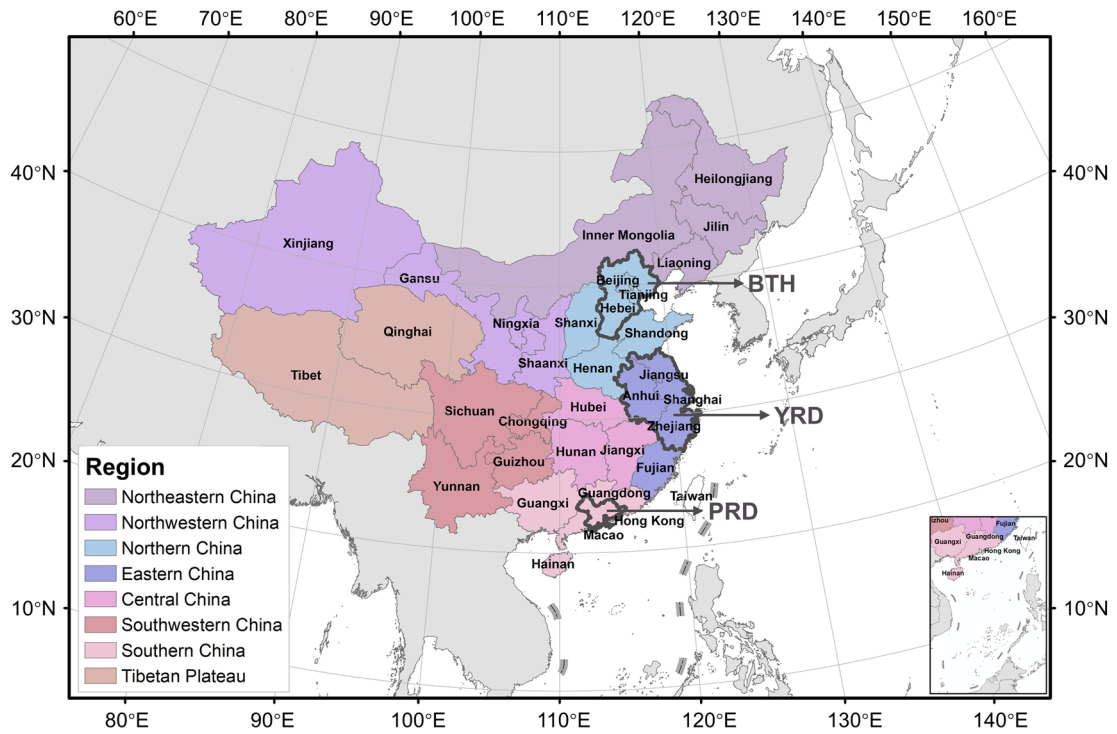
	China	BTH	YRD	PRD
	Emissions (Tg)	Emission intensity (Gg grid ⁻¹)		
2020s	33.6	1.4	4.6	8.7
2060s	43.4	1.7	5.7	10.7
Growth rate	29.2 %	21.4 %	23.9 %	23.0 %

1091

1092

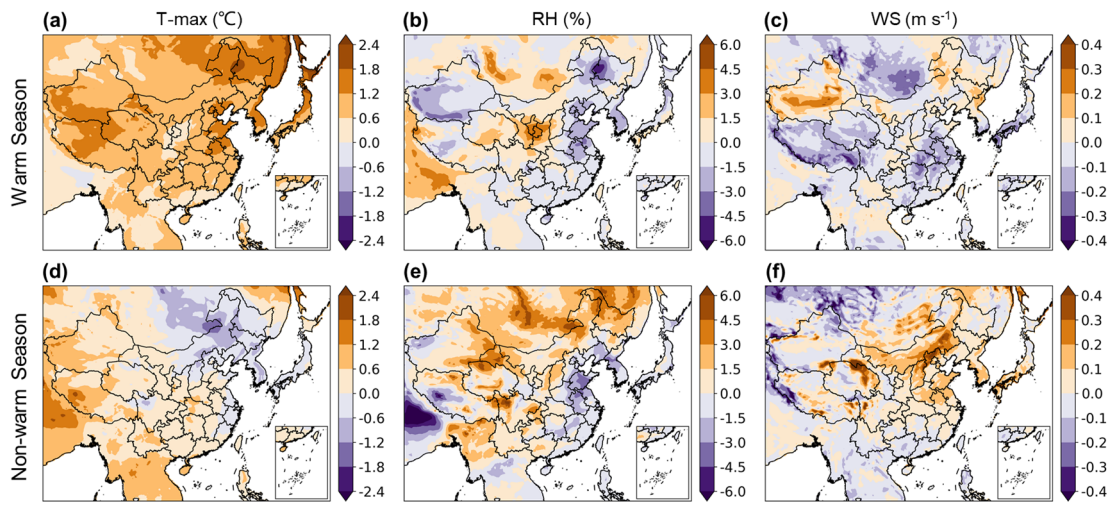
1093 **FIGURES**

1094 **Figure 1**



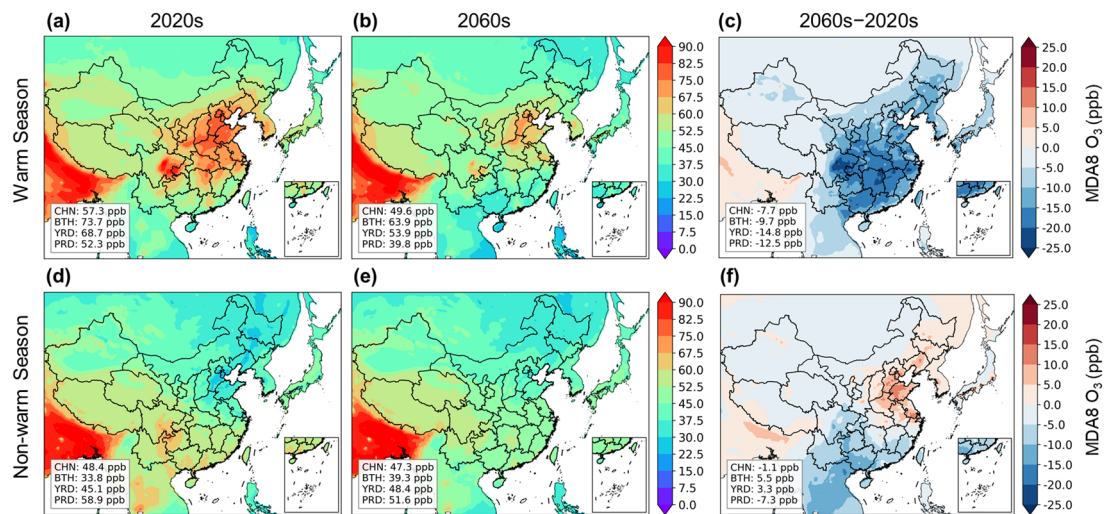
1095
1096

1097 **Figure 2**



1098
1099

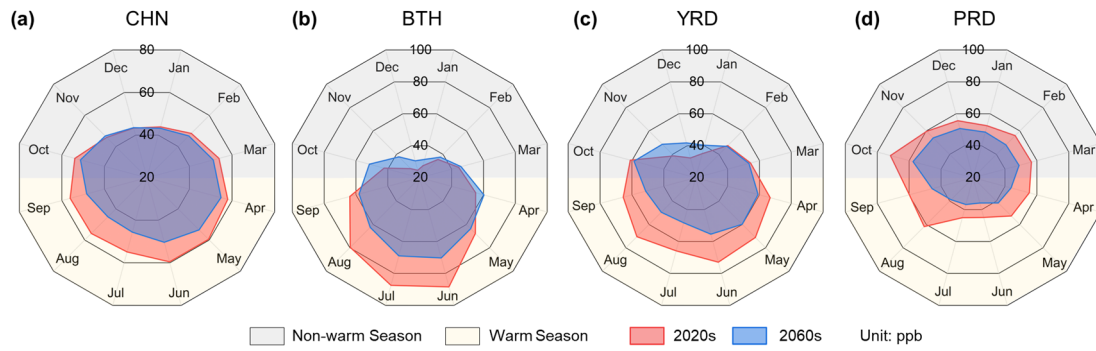
1100 **Figure 3**



1101

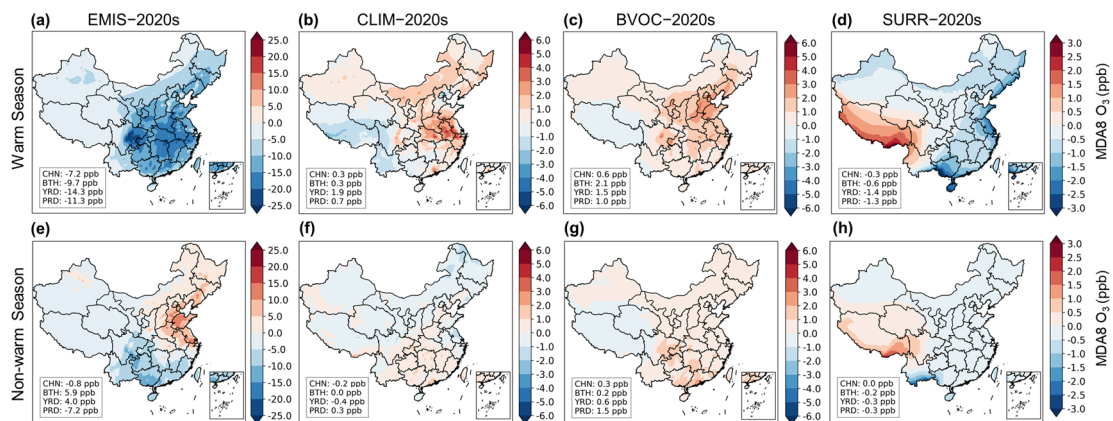
1102

1103 **Figure 4**



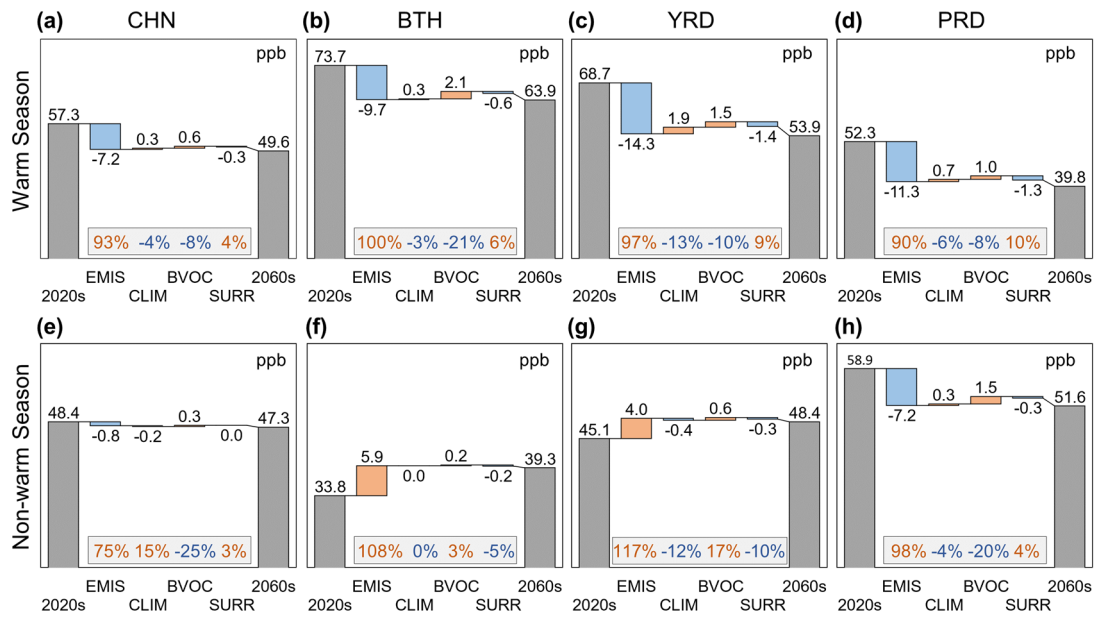
1104

1105



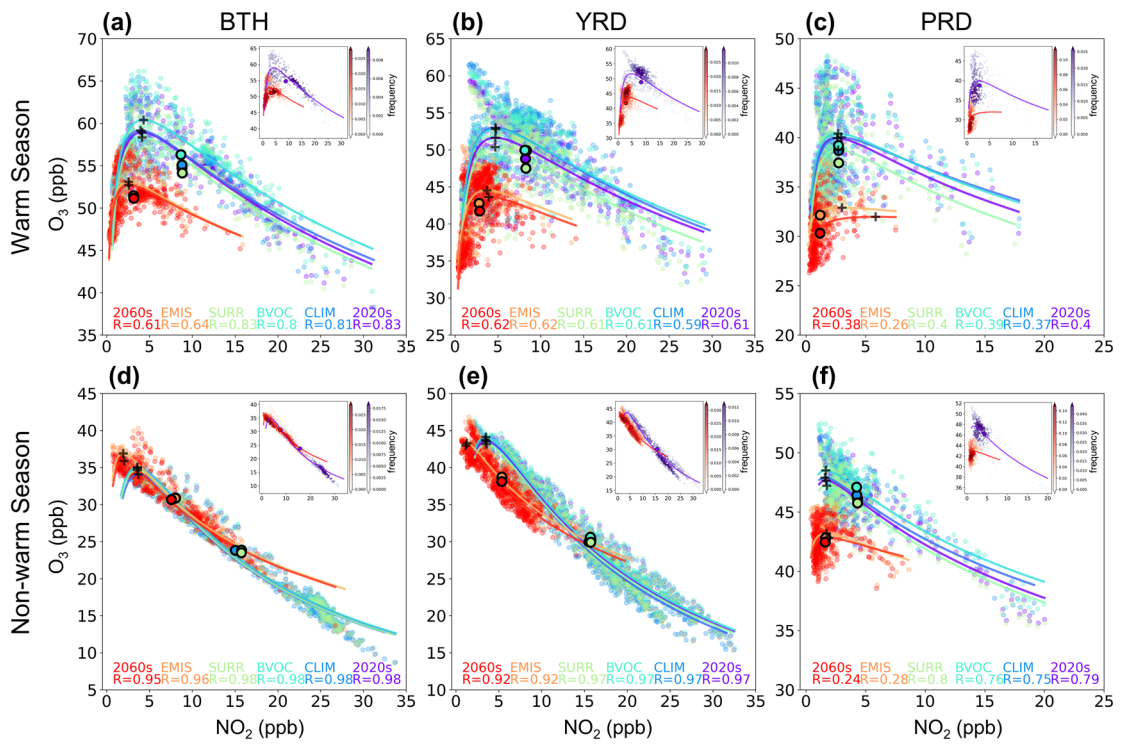
1107
1108

1109 **Figure 6**



1110

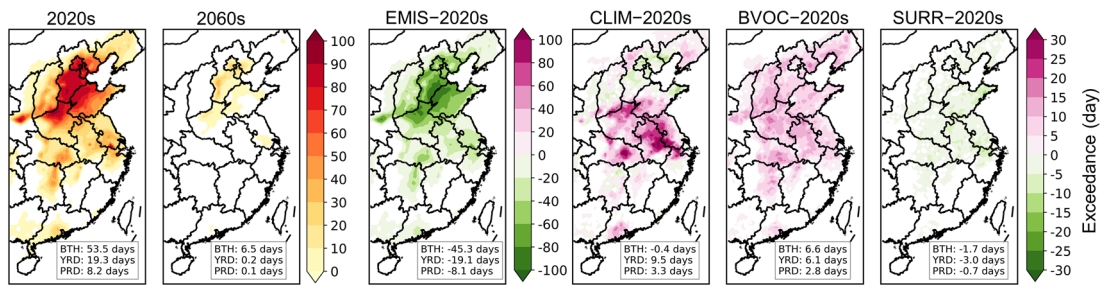
1111



1113
1114

1115 **Figure 8**

1116



1 **Supplement of**
2 **Investigating the response of China's surface ozone concentration to**
3 **the future changes of multiple factors**

4 Jinya Yang¹, Yutong Wang¹, Lei Zhang^{1,2}, Yu Zhao^{1,2*}

5
6 1. State Key Laboratory of Pollution Control and Resource Reuse, School of
7 Environment, Nanjing University, 163 Xianlin Rd., Nanjing, Jiangsu 210023, China

8 2. Jiangsu Collaborative Innovation Center of Atmospheric Environment and
9 Equipment Technology (CICAET), Nanjing University of Information Science and
10 Technology, Jiangsu 210044, China

11

12 *Corresponding author: Yu Zhao

13 Phone: 86-25-89680650; email: yuzhao@nju.edu.cn

14

15

16 **Number of tables: [23](#) Number of figures: 7**

17 **Table list**

18 Table S1 Statistical metrics for comparison between the observed and simulated
19 monthly average meteorological variables and MDA8 O₃ in 2020. OBS is mean of
20 observation, SIM is mean of simulation, and Bias is mean bias between SIM and OBS.
21 R, NMB, NME and IOA refers to the correlation coefficient, normalized mean bias,
22 normalized mean error and index of agreement between SIM and OBS, respectively.

23 Table S2 Comparison of BVOCs estimates between this study and previous estimations
24 for 2020.

25 [Table S3 Coefficients of variation \(CVs\) for simulated O₃ concentrations within five-](#)
26 [year simulations for the whole country \(CHN\) and selected developed regions \(BTH,](#)
27 [YRD, and PRD\).](#)

28 **Figure list**

29 Figure S1 The NO_x and NMVOCs emissions in 2020 and 2060 for the surrounding
30 areas within the modelling domain but excluding Chinese mainland (SURR), Chinese
31 mainland (CHN), as well as the three regions. Data illustrated are obtained from MEIC
32 for 2020 and DPEC for 2060 within Chinese mainland, and SSP dataset for the rest.

33 Figure S2 Spatial distribution of the observation (circles) and simulation (shaded) of
34 monthly average MDA8 O₃ in 2020 across China.

35 Figure S3 The spatial distribution of BVOCs emissions of the 2020s and the difference
36 between the 2060s and 2020s.

37 Figure S4 The distribution of O₃ seasons across China and the three regions, and the
38 top six months with the highest levels of O₃ pollution are covered by darker color. Note
39 that there is discrepancy between simulation and observation in PRD for 2020s.
40 February and March are simulated as two of the six most polluted months, while the
41 observation indicates April and May.

42 Figure S5 The emission reduction rates for the two precursors during 2020 and 2060
43 over China and the three regions.

44 Figure S6 Simulation and projection of hourly O₃ and O_x in the 2020s and 2060s over
45 China and the three regions.

46 Figure S7 Projected seasonal O₃ exceedance over the east of China in the 2020s and
47 2060s, and the exceedance changes when the four factors at 2060s level.

48 **Tables**

49 Table S1 Statistical metrics for comparison between the observed and simulated
 50 monthly average meteorological variables and MDA8 O₃ in 2020. OBS is mean of
 51 observation, SIM is mean of simulation, and Bias is mean bias between SIM and OBS. R,
 52 NMB, NME and IOA refers to the correlation coefficient, normalized mean bias,
 53 normalized mean error and index of agreement between SIM and OBS, respectively.

Variables	OBS	SIM	Bias	R	NMB	NME	IOA	
T2 (°C)	13.21	12.53	-0.6 9	0.9 6	-5.20 %	17.65 %	0.98	
WS (m s ⁻¹)	2.60	4.02	1.41	0.5 1	54.21 %	60.04 %	0.57	
WD (°)	175.75	174.78	-0.9 7	0.5 1	-0.55 %	18.40 %	0.72	
RH (%)	65.25	66.17	0.92	0.7 8	1.41 %	12.78 %	0.88	
MDA 8 O ₃ (ppb)	Warm season	57.45	8.11 6	8.11	0.7 1	14.12 %	16.33 %	0.74
	Non- warm season	38.67	4.21 8	4.21	0.3 2	10.90 %	25.48 %	0.49

54

55 Table S2 Comparison of BVOCs estimates between this study and previous estimations.

Species	Period	Annual emission (Tg)	Reference
Total BVOCs	2020s	33.55	This study
	2015–2019	29.28±0.91	Ma et al. (2021)
	2015–2019	31.42±0.95	Ma et al. (2021)
	2008–2018	54.60	Li et al. (2020)
	2001–2016	34.27	Wang et al. (2021)
	2017	23.54	Wu et al. (2020)
Isoprene	2020s	21.08	This study
	2015–2019	13.88±0.57	Ma et al. (2021)
	2015–2019	14.29±0.54	Ma et al. (2021)
	2008–2018	29.30	Li et al. (2020)
	2001–2016	15.94	Wang et al. (2021)
	2017	13.30	Wu et al. (2020)
Terpenes	2020s	3.30	This study
	2015–2019	5.28±0.12	Ma et al. (2021)
	2015–2019	4.77±0.11	Ma et al. (2021)
	2017	3.09	Wu et al. (2020)

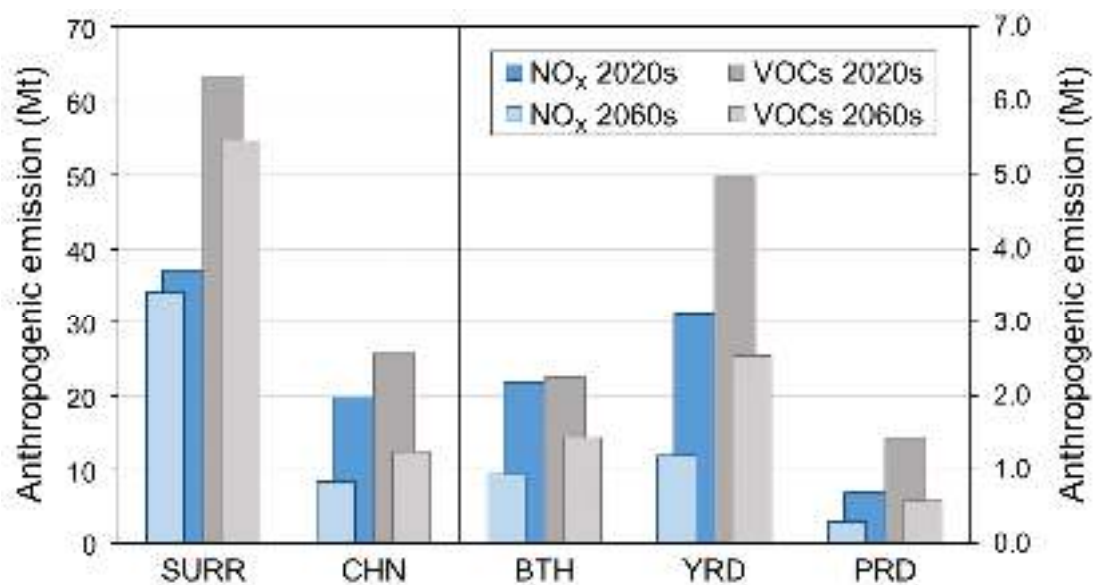
56

57 [Table S3 Coefficients of variation \(CVs\) for simulated O₃ concentrations within five-](#)
 58 [year simulations for the whole country \(CHN\) and selected developed regions \(BTH,](#)
 59 [YRD, and PRD\).](#)

<u>Simulation</u>	<u>Warm Season</u>				<u>Non-warm Season</u>			
	<u>CHN</u>	<u>BTH</u>	<u>YRD</u>	<u>PRD</u>	<u>CHN</u>	<u>BTH</u>	<u>YRD</u>	<u>PRD</u>
<u>2020s</u>	<u>2.6 %</u>	<u>5.7 %</u>	<u>1.8 %</u>	<u>4.0 %</u>	<u>1.4 %</u>	<u>0.9 %</u>	<u>2.7 %</u>	<u>3.8 %</u>
<u>2060s</u>	<u>1.5 %</u>	<u>4.0 %</u>	<u>2.2 %</u>	<u>5.6 %</u>	<u>0.8 %</u>	<u>1.3 %</u>	<u>2.1 %</u>	<u>3.4 %</u>
<u>CLIM</u>	<u>1.9 %</u>	<u>5.9 %</u>	<u>2.5 %</u>	<u>6.5 %</u>	<u>1.1 %</u>	<u>1.6 %</u>	<u>4.1 %</u>	<u>3.8 %</u>
<u>EMIS</u>	<u>2.2 %</u>	<u>3.3 %</u>	<u>2.2 %</u>	<u>3.7 %</u>	<u>1.4 %</u>	<u>1.4 %</u>	<u>1.5 %</u>	<u>2.5 %</u>
<u>BVOC</u>	<u>2.6 %</u>	<u>5.0 %</u>	<u>2.0 %</u>	<u>4.3 %</u>	<u>1.4 %</u>	<u>1.0 %</u>	<u>2.3 %</u>	<u>3.4 %</u>
<u>SURR</u>	<u>2.7 %</u>	<u>5.8 %</u>	<u>1.7 %</u>	<u>4.1 %</u>	<u>1.5 %</u>	<u>0.9 %</u>	<u>2.7 %</u>	<u>3.9 %</u>

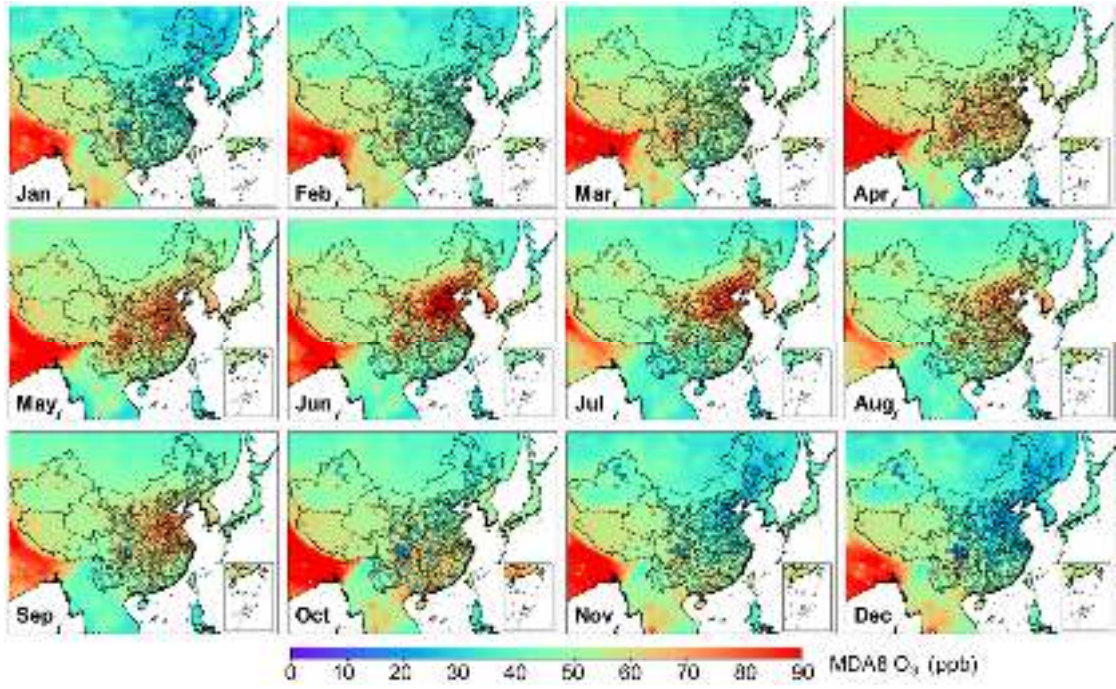
60

61 **Figures**



62 Figure S1 The NO_x and NMVOCs emissions in 2020 and 2060 for the surrounding
63 areas within the modelling domain but excluding Chinese mainland (SURR), Chinese
64 mainland (CHN), as well as the three regions. Data illustrated are obtained from MEIC
65 for 2020 and DPEC for 2060 within Chinese mainland, and SSP dataset for the rest.

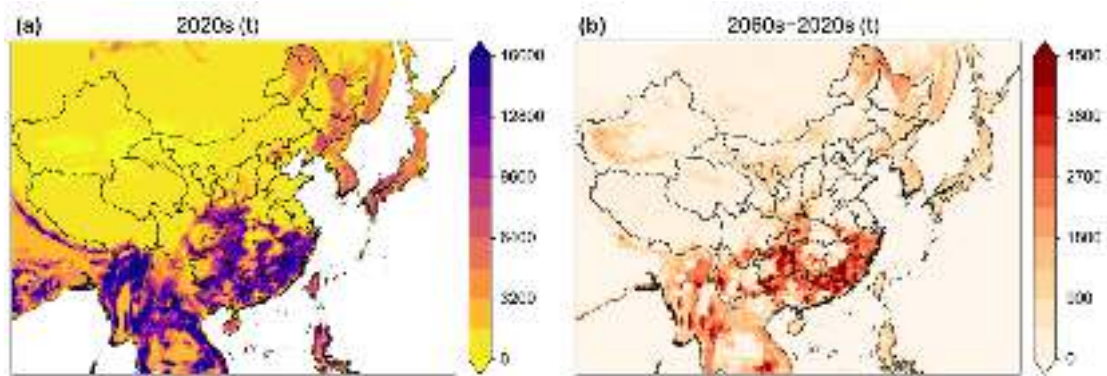
66



67

68 Figure S2 Spatial distribution of the observation (circles) and simulation (shaded) of
 69 monthly average MDA8 O₃ in 2020 across China.

70

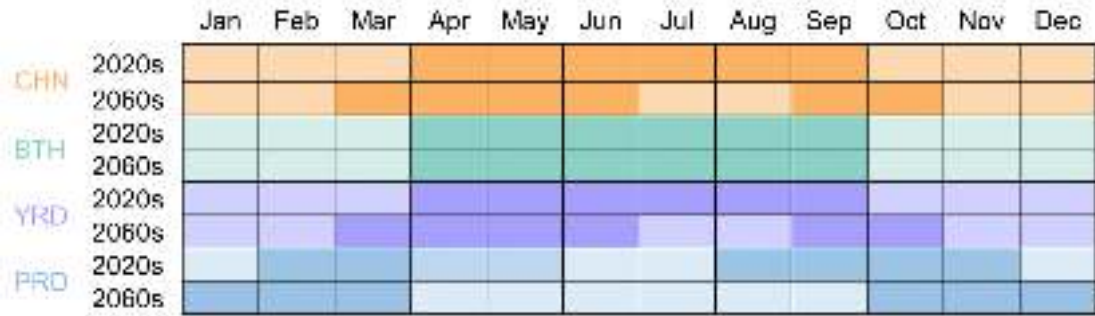


71

72 Figure S3 The spatial distribution of BVOCs emissions of the 2020s and the difference
73 between the 2060s and 2020s.

74

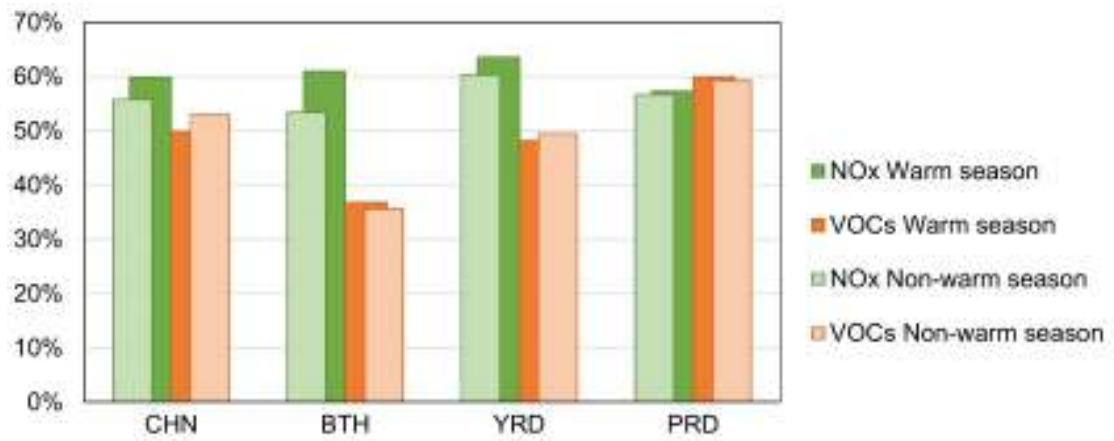
75



76

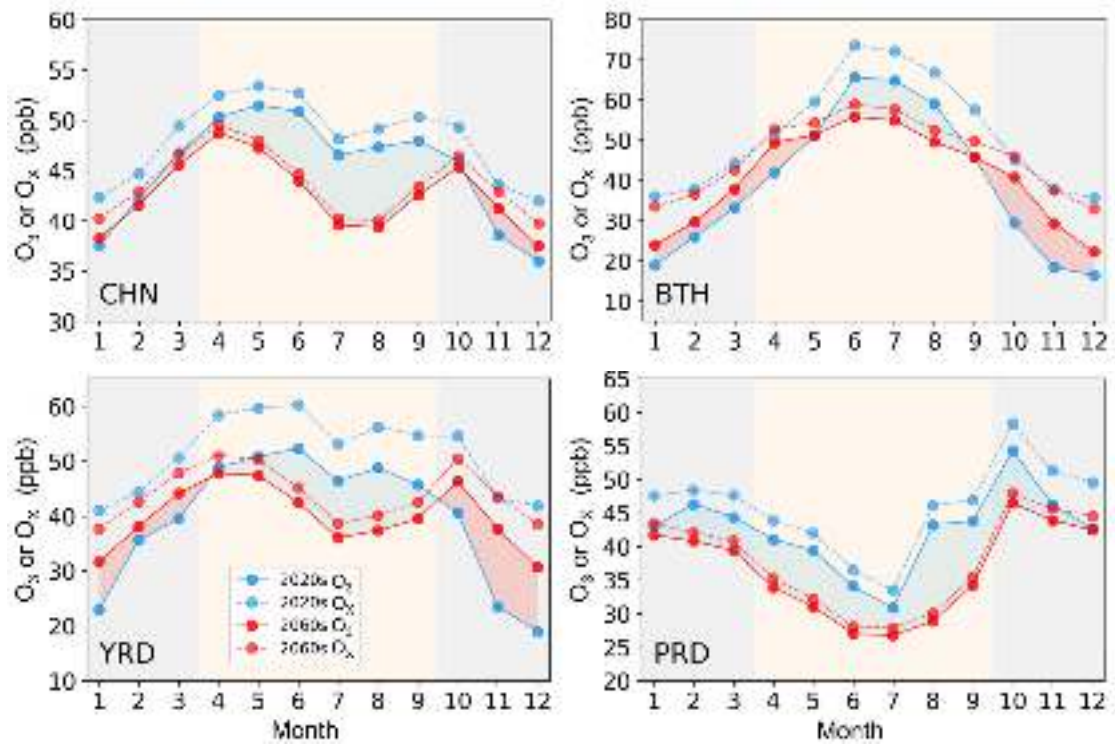
77 Figure S4 The distribution of O₃ seasons across China and the three regions, and the
 78 top six months with the highest levels of O₃ pollution are covered by darker color. Note
 79 that there is discrepancy between simulation and observation in PRD for 2020s.
 80 February and March are simulated as two of the six most polluted months, while the
 81 observation indicates April and May.

82



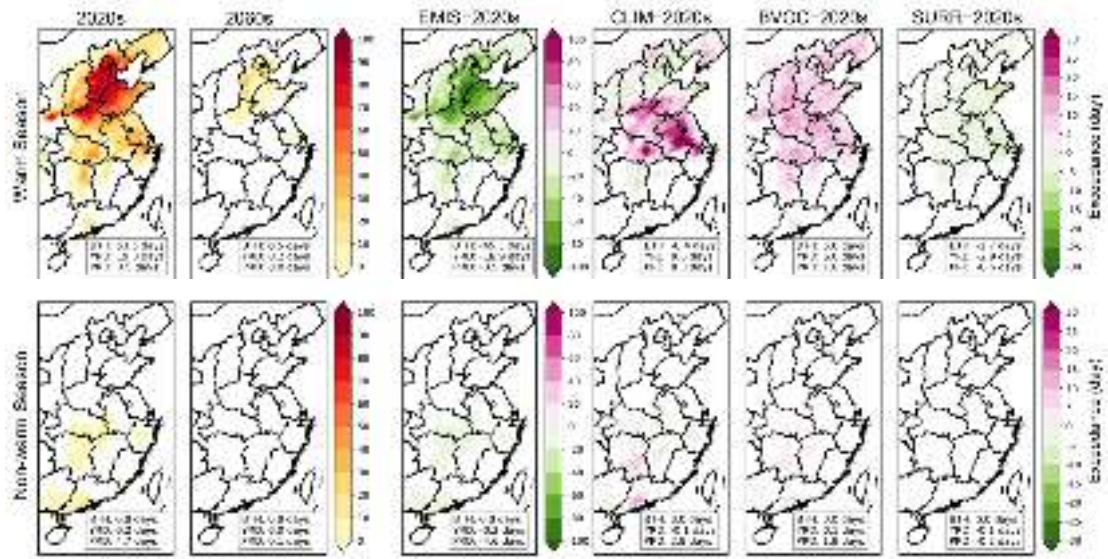
83 Figure S5 The emission reduction rates for the two precursors during 2020 and 2060
 84 over China and the three regions.

85



86 Figure S6 Simulation and projection of hourly O₃ and O_x in the 2020s and 2060s over
 87 China and the three regions.

88



89 Figure S7 Projected seasonal O₃ exceedance over the east of China in the 2020s and
 90 2060s, and the exceedance changes when the four factors at 2060s level.

91

92 **References**

- 93 Li, L., Yang, W., Xie, S., and Wu, Y.: Estimations and uncertainty of biogenic volatile
94 organic compound emission inventory in China for 2008-2018, *Science of the Total*
95 *Environment*, 733, 139301, 10.1016/j.scitotenv.2020.139301, 2020.
- 96 Ma, M., Gao, Y., Ding, A., Su, H., Liao, H., Wang, S., Wang, X., Zhao, B., Zhang, S.,
97 Fu, P., Guenther, A. B., Wang, M., Li, S., Chu, B., Yao, X., and Gao, H.: Development
98 and Assessment of a High-Resolution Biogenic Emission Inventory from Urban Green
99 Spaces in China, *Environmental Science & Technology*, 10.1021/acs.est.1c06170, 2021.
- 100 Wang, H., Wu, Q., Guenther, A. B., Yang, X., Wang, L., Xiao, T., Li, J., Feng, J., Xu,
101 Q., and Cheng, H.: A long-term estimation of biogenic volatile organic compound
102 (BVOC) emission in China from 2001–2016: the roles of land cover change and climate
103 variability, *Atmospheric Chemistry and Physics*, 21, 4825-4848, 10.5194/acp-21-4825-
104 2021, 2021.
- 105 Wu, K., Yang, X., Chen, D., Gu, S., Lu, Y., Jiang, Q., Wang, K., Ou, Y., Qian, Y., Shao,
106 P., and Lu, S.: Estimation of biogenic VOC emissions and their corresponding impact
107 on ozone and secondary organic aerosol formation in China, *Atmospheric Research*,
108 231, 10.1016/j.atmosres.2019.104656, 2020.